

*We thank the two reviewers for their constructive and helpful comments. We are pleased that both authors believe that the paper is well-structured and written, recommending publication after minor revisions. In the following we address the comments and suggestions by the reviewer's point-by-point.*

## **Reviewer 1**

General remark 1: Most importantly, I think it would be good to present a general "expectation" based on the forward modelling more clearly. Under "normal" neutral stratification of the surface layer emissions are taken up by the atmosphere and vertically (and horizontally) dispersed. Thus, the concentration will generally increase relative to the background (S2), and in ideal circumstances with homogeneous emissions, S3 will generally be higher in concentration than S1. Also, the concentration will not increase linearly with distance, since vertical dispersion takes place. A clear description of this concept will help the reader to understand the need for non-homogeneous emissions in Period 2.

*-> authors: The reviewer makes a good point, we have added a few sentences more to further clarify the inverse dispersion theory in section 2.4.*

General remark 2: the formulas sometimes lack units

*-> authors: We have addressed this remark in the revised manuscript (see comment 6).*

General remark 3: A third remark concerns the choice of Period 2 for the Q/EF estimates. This period is characterized by a more uncertain background. The reason given (Period 1 is too short) I find not convincing. More emphasis should be placed on Period 1, which seems more consistent from a methodological point of view.

*-> authors: The emission estimates made during Period 1 are not suitable for an emission factor due to the high likelihood that emissions continued to occur from the plot long after the Period 1 measurements ended. Therefore there was a significant fraction of emissions from excretions deposited to the field during Period 1 that were not captured by the Period 1 downwind concentration measurements, because the Period 2 grazing period began immediately afterwards and the concentration receptors had been moved to different field boundaries. An emission factor based on the Period 1 emissions would largely underestimate the total emissions from grazing due to the Period 1 receptors "missing" the delayed emissions from cattle excretions. After the Period 2 grazing period, the miniDOAS receptors were left in place for several days, this allowed the Period 2 receptors to capture residual emissions from the excretions, and thus provide a more complete estimate of the total emissions from grazing. It is for this reason that we believe that a Period 2 emission factor is more representative. However, the emissions from both periods 1 and 2 are presented, along with emission factors expressed in multiple ways for both. This reasoning for the selection of the Period 2 emission factor is explained thoroughly in the discussion section.*

Comment 1: Page 3, line 71 - maybe redefine in main text.

*-> authors: Done.*

Comment 2: Page 4, line 131 - This sentence is extremely vague. It forces readers to go to the Sintermann publication. It is unclear what the slope is in this context. Please be more specific here.

-> authors: *This sentence has been rephrased for clarification.*

Comment 3: Page 5, line 153 - So, why would you need temperature at 1.4m and 2m. Are these compared, or is this second measurement more specific?

-> authors: *The measurement at 1.4m height is the fast temperature measurement component of the sonic anemometer, logged at 20Hz and later processed by eddy covariance software. The temperature and relative humidity sensor at 2m height (HMP45C, Campbell Scientific) is the better sensor for recording changes in ambient temperature (more accurate absolute temperature readings). This has now been clarified in the text.*

Comment 4: Page 6, line 174 - The description provided here does not clarify the reason for using the absolute value of  $2/w_0$  in the calculation. Either refer again to the Flesch paper (for more details ....), or provide a more detailed description here.

-> authors: *Done, we have now clarified the  $w_0$  term in section 2.4.*

Comment 5: Page 6, line 176 - Also here, it remains unclear how these parameters influence the source estimate. At least you should mention here that the vertical mixing depth (i.e. the turbulence) is the prime factor in linking a concentration enhancement to a source strength.

-> authors: *We have addressed this comment in the revisions following general remark 1.*

Comment 6: Page 7, line 236 - Is T in celcius? Please provide units for alpha and beta.

-> authors: *Units for T and beta are added, alpha is unitless.*

Comment 7: Page 8, line 258 - I think the authors are aware of the accepted vision that managed grasslands have bi-directional exchange of ammonia: at periods of high temperatures emissions may occur, while at other periods emissions are monitored over the same field. This view has led to bi-directional exchange models (Fowler ...,... Kruit, ). The authors should at least mention this in the paragraph. and mention that the current implementation is a simplification of what is known.

1. Kruit, R. J. W. et al. Modeling the surface-atmosphere exchange of ammonia. Atmos Environ {44}, {945–957} (2010).

1. Fowler, D. et al. Atmospheric composition change: Ecosystems–Atmosphere interactions. Atmos Environ 43, 5193–5267 (2009).

-> authors: *We have added a few sentences to section 2.6 explaining that surface-atmosphere exchange is bi-directional and the uni-directional resistance model approach is a simplification. We thank the reviewer for the references provided.*

Comment 8: Page 9, line 285 - I think it is instrumental to give units of the variables. RH in %, T in Kelvin? Cb in ug/m3? u in m/s?

-> authors: Units have been added to equation 5.

Comment 9: Page 9, line 289 - Should QS5 in figure 4 be QS3?

-> authors: Yes, this mistake has now been corrected.

Comment 10: Page 10, line 239 - Here it seems odd to me that the range line in the figure on May 27 is above the lue and the black (implying negative emissions). Would be logical to set cb to the minimum of the measured concentrations.

-> authors: The predicted background concentration (Figure 6, orange line) does not agree strongly with the measured background concentration. The predicted Cb exceeds the downwind S3 concentration measurements (blue line) on May 27 as a result of this. However, on May 27 we had active upwind concentration measurements (S2, red line), thus the measured Cb was used in the emission estimates. The sensitivity of the emission estimates to Cb uncertainty is explored in detail (Table 4, Section 4.4.2).

## Reviewer 2

Chapter 2.2: Ammonia measurements. The authors could give some numbers regarding the quality of the measurements of the paper of Sintermann et al. 2016, e.g. for the calibration procedure and the comparison of the 3 miniDOAS systems.

-> authors: We have now stated the random uncertainty of the NH3 measurements (1.4% of the concentration levels). The comparison of the three miniDOAS systems gave a coefficient of variation of 3.4%, this is also shown in Chapter 2.2

Page 8, Line 252: Give standard deviation of Rc value, as the individual points show large variability in the figure.

-> authors: Done, the standard deviations have been added.

Line 446: unpublished data could be shown in the supplements

-> authors: The data we are referring to here is the 1 minute miniDOAS measurement intercomparison period where the three systems were run in parallel. Sintermann et al. (2016) present these data, however the S1 sensor was omitted because it did not have the same technical specification as the S2 and S3 sensors which had been upgraded with new components. In our study we use the data from all three miniDOAS systems, thus with this small difference we do not believe it is necessary to publish the same data twice, as Sintermann et al. (2016) paper analyses the inter-comparison period in detail. We present an updated coefficient of variation value to reflect the intercomparison of all 3 systems (3.4%). We have added a sentence to this section to clarify the inter-comparison data published by Sintermann et al.

Line 498: Replace QS5 by QS3 (also in Figure 4 and 6)

-> *authors: Done*

Figure 4: Add cattle presence (like figure 6) and change QS5 to QS3

-> *authors: QS5 has now been changed to QS3, we have added a statement in the figure caption stating that the cattle were present for the entire time period shown.*

## List of relevant changes

1. Further explanation has been given to the inverse dispersion modelling theory, section 2.4
2. Units have been added to equations 4, 5 & 6
3. The Sintermann et al. (2016) miniDOAS comparison experiment has further described and the random uncertainty of the miniDOAS system measurements been given to show the instrumental precision.
4. The concept of bi-directional NH<sub>3</sub> exchange has been introduced to explain the simplifications involved with the uni-directional resistance model used by the bLS-R model to simulate deposition.
5. The standard deviations of the COTAG canopy resistance measurements are now given (section 2.6).
6. A mistake has been corrected in figure 4 and 6 where the QS3 sensor was wrongly labelled as QS5.

1 **Ammonia emissions from a grazed field estimated by**  
2 **miniDOAS measurements and inverse dispersion modelling**

3 Michael Bell<sup>1</sup>, Christophe Flechard<sup>1</sup>, Yannick Fauvel<sup>1</sup>, Christoph Häni<sup>2</sup>, Jörg Sintermann<sup>3a</sup>,  
4 Markus Jocher<sup>3</sup>, Harald Menzi<sup>4</sup>, Arjan Hensen<sup>5</sup>, Albrecht Neftel<sup>3b</sup>

5 <sup>1</sup>INRA, Agrocampus Ouest, UMR 1069 SAS, Rennes, France

6 <sup>2</sup>Bern University of Applied Sciences, School of Agricultural, Forest and Food Sciences, CH-3052 Zollikofen,  
7 Switzerland

8 <sup>3</sup>Agroscope - Institute for Sustainability Science, Zürich, Switzerland

9 <sup>4</sup>Federal Research Station Agroscope, Inst. For Livestock Sciences, 1725 Posieux, Switzerland

10 <sup>5</sup>Energy research Centre of the Netherlands (ECN), Petten, The Netherlands

11 <sup>a</sup>now at AWEL, Zürich, Switzerland

12 <sup>b</sup>now at Neftel research Expertise, C -3033 Wohlen b. Bern, Switzerland

13

14 *Correspondence to:* Michael Bell (michael.bell@inra.fr)

15

## 16 Abstract

17 Ammonia (NH<sub>3</sub>) fluxes were estimated from a field being grazed by dairy cattle during spring, by applying a  
18 backward-Lagrangian Stochastic model (bLS) model combined with horizontal concentration gradients  
19 measured across the field. Continuous concentration measurements at field boundaries were made by open-path  
20 miniDOAS (differential optical absorption spectroscopy) instruments, during the cattle's presence and for 6  
21 subsequent days. The deposition of emitted NH<sub>3</sub> to 'clean' patches on the field was also simulated, allowing  
22 both 'net' and 'gross' emission estimates, where the dry deposition velocity ( $v_d$ ) was predicted by a canopy  
23 resistance ( $R_c$ ) model developed from local NH<sub>3</sub> flux and meteorological measurements. Estimated emissions  
24 peaked during grazing and decreased after the cattle had left the field, while control on emissions was observed  
25 from covariance with temperature, wind speed and humidity/wetness measurements made on the field, revealing  
26 a diurnal emission profile. Large concentration differences were observed between downwind receptors, due to  
27 spatially heterogeneous emission patterns. This was likely caused by uneven cattle distribution and a low  
28 grazing density, where 'hotspots' of emissions would arise as the cattle grouped in certain areas, such as around  
29 the water trough. The spatial complexity was accounted for by separating the model source area into sub-  
30 sections, and optimising individual source area coefficients to measured concentrations. The background  
31 concentration was the greatest source of uncertainty, and based on a sensitivity/uncertainty analysis the overall  
32 uncertainty associated with derived emission factors from this study is at least 30-40%.  
33 Emission factors can be expressed as  $6 \pm 2$  g NH<sub>3</sub> cow<sup>-1</sup> day<sup>-1</sup>, or  $9 \pm 3\%$  of excreted urine-N emitted as NH<sub>3</sub>,  
34 when deposition is not simulated, and  $7 \pm 2$  g NH<sub>3</sub> cow<sup>-1</sup> day<sup>-1</sup>, or  $10 \pm 3\%$  excreted urine-N emitted as NH<sub>3</sub>  
35 when deposition is included in the gross emission model. The results suggest that around  $14 \pm 4\%$  of emitted  
36 NH<sub>3</sub> was deposited to patches within the field that were not affected by urine or dung.

## 37 1. Introduction

38 Over 90% of anthropogenic ammonia (NH<sub>3</sub>) emissions in Europe have agricultural sources (Erisman et al.,  
39 2008; Reidy et al., 2008; Hertel et al., 2011), 70-90% of which have been estimated to be produced by livestock  
40 (Pain et al., 1998; Hutchings et al., 2001). In addition to decreasing nitrogen efficiency for farming systems, the  
41 volatilisation of NH<sub>3</sub> from agricultural areas is a principal factor in the formation of fine fraction secondary  
42 aerosols due to its reactions with nitric and sulphuric acids in the atmosphere, and upon deposition is linked to  
43 acidification and eutrophication of natural ecosystems (Sutton et al., 2011). Following the application of urine  
44 and dung to the soil surface by grazing livestock, urea is microbially converted to NH<sub>3</sub> which is volatilised at  
45 rates which vary extensively depending on soil and canopy layer properties, weather, and culture conditions  
46 (Laubach et al., 2013a). It has been estimated that 75-90% of the N ingested by a grazing cow is metabolised  
47 inefficiently and returned by excreta to the grazing paddocks, of which over 70% is returned as urine  
48 (Whitehead, 1995; Zaman et al., 2009). NH<sub>3</sub> emissions have been measured from cattle urine patches at the ratio  
49 of 7-25.7% of excreted urine nitrogen (N) for grazed pastures (Jarvis et al., 1989; Ryden et al., 1987; Laubach et  
50 al., 2012; 2013a), and measurements from sheep urine patches in summer-winter experiments have suggested  
51 emissions which represent 12.2–22.2% of excreted urine-N (Sherlock and Goh, 1984).

52 Methods for estimating emissions from grazed pastures include micrometeorological methods, where profiles of  
53 concentration and wind speed are measured at one or more points downwind from the source, allowing fluxes to

54 be calculated using the theory of turbulent transport in the atmospheric surface layer (Laubach et al., 2012).  
55 Dynamic chambers or movable wind tunnels may be used to estimate emissions from simulated grazing in the  
56 laboratory or the field (Sommer et al., 2001). However enclosure measurements may not always be  
57 representative of emissions at the field scale (Genermont and Cellier, 1997; Sintermann et al., 2012). The  
58 inverse dispersion method concerns the inferring of the atmospheric emission rate ( $Q$ ) of localised gas sources  
59 from the excess concentration ( $\Delta C$ ) they cause above background, by modelling the  $\Delta C/Q$  relationship for a  
60 given ~~measurement setup under the existing~~source-receptor configuration and meteorological state (Flesch et al.,  
61 2004; Flesch et al., 2014).

62 The local dry deposition of  $\text{NH}_3$  within the grazed field is an important consideration to make, as in contrast to  
63 other pollutants a significant proportion may be deposited locally (e.g. Loubet et al., 2009). The proportion of  
64 deposited  $\text{NH}_3$  is sensitive to multiple parameters, including the source height, wind speed, atmospheric  
65 stability, land cover type and the numerous specific surface parameters therein (e.g. Sutton et al. 1993). This  
66 leads to modelling results that vary widely, with local recapture ranging from 2% to 60% within 2km from the  
67 source (Loubet et al., 2006, Asman et al., 1998). Accordingly, the modelling of  $\text{NH}_3$  deposition can be a  
68 challenging undertaking, with models ranging from simple steady-state canopy resistance models to dynamic,  
69 bi-directional, multi-layer and multi-process chemical species schemes (Flechard et al., 2013). Local-scale  
70 deposition models may ignore the wet deposition process, as dry deposition is most likely the dominant ~~dry~~  
71 deposition mechanism near sources (Loubet et al., 2009).

72 In this study, a bLS (backward Lagrangian Stochastic) dispersion model with a coupled dry deposition scheme  
73 has been applied to estimate the  $\text{NH}_3$  emissions from a field being grazed by dairy cows, using the horizontal  
74 concentration gradients measured across the field by three open-path miniDOAS instruments (Sintermann et al.,  
75 2016; Volten et al., 2012). The open-path measurement system is to considerable benefit, as most techniques to  
76 measure atmospheric  $\text{NH}_3$  are sampling techniques and therefore involve inlet contact with the highly adhesive  
77  $\text{NH}_3$ , which may slow response times and lead to interaction with water molecules and interference by  
78 ammonium aerosols dissociating on tubes or filters (e.g. von Bobruzki et al., 2010). The miniDOAS system is a  
79 comparatively interference-free measurement technique, since it utilises the wavelength-dependent UV-light  
80 absorption of  $\text{NH}_3$  over an open light path. The system also has capacity for long-term fast response continuous  
81 measurements, and a broad measurement path which makes the miniDOAS a well-suited concentration  
82 ~~receptors~~receptor for monitoring the fluctuations in  $\text{NH}_3$  concentrations across field boundaries.

83 The objectives of our study were: (1) to evaluate the  $\text{NH}_3$  emissions from cattle grazing using the bLS  
84 dispersion technique and contribute towards an emission factor, as there is a limited number of existing  
85 measurements, (2) to simulate the degree of re-deposition that occurs within the field, and (3) evaluate the  
86 application of the bLS technique and the miniDOAS measurement system to derive  $\text{NH}_3$  fluxes from  
87 agricultural diffuse sources such as grazing. ~~The bLS model assumes a homogenous source area, therefore it~~It  
88 was assumed that emission estimates would be insensitive to irregular cattle distribution and excretion patterns.  
89 The measurement of concentration gradients across grazed fields is challenging, as downwind concentration  
90 levels may not rise far above background as is the case with stronger sources, such as applied slurry. Therefore,  
91 this is an exercise which requires precise and continuous measurements from two or more sensors to evaluate  
92 ( $\Delta C$ ). However, the method is also ~~nonintrusive~~non-intrusive and is not labour intensive, and can provide

93 continuous emission estimates over long or short time periods if the conditions and experimental design are in  
94 agreement.

## 95 2. Methods

### 96 2.1 Site description and experimental design

97 The experiments were conducted from 18-29 May 2015, on a rectangular grazing pasture of about two hectares  
98 at the INRA-Méjusseaume dairy research experimental farm in NW France (48-~~11704~~, ~~—~~°07'01.3"N  
99 | ~~1.79736~~°47'50.5"W). The site was flat and benefited from a lack of wind-disturbing elements within 100m of  
100 the field boundaries (e.g. trees, buildings or other protruding elements). The cattle were not given additional  
101 feed to supplement grazing (mixed grass sward rich in *Lolium perenne*). The field had been previously grazed  
102 one month prior (16-27 May 2015) to the beginning of the experiment, and mineral fertiliser had been applied  
103 | on 31/03. During measurement Period 1, 25 cows were ~~allowed to graze~~ grazing within the southwestern section  
104 of the field (Area D, Figure 1) from 08:00 18/05 - 15:00 20/05 UTC (28 hours grazing), with three sets of  
105 miniDOAS open-path sensors and placed along the northern, western and eastern boundaries. The miniDOAS  
106 sensors were placed to optimise the measurement of ( $\Delta C$ ) across the field after reviewing wind directions  
107 forecast for the week ahead. The miniDOAS sensors have been given the names S1, S2 and S3, where the S2  
108 sensor was placed upwind of the grazed field while the S1 and S3 sensors were placed at downwind locations.  
109 During Period 2, the whole field (Areas A, B, C, D) was opened for 44 grazing cattle, with the cattle present on  
110 the field from 10:00 20/05 – 05:00 23/05 (60 hours grazing), while the miniDOAS sensors were left in place to  
111 measure residual emissions from 23-29/05. The cattle were removed from the field for milking during both  
112 periods for roughly one hour twice per day. As the field area during Period 2 was much larger, the S2 and S3  
113 miniDOAS sensors were moved to the north-western and south-eastern field boundaries respectively, leaving  
114 the three miniDOAS paths in-line with a NW-SE transect of the field (Figure 1). The grazing densities during  
115 Periods 1 and 2 were 44 and 22 cattle ha<sup>-1</sup>, respectively.

### 116 2.2 Ammonia measurements

117 The DOAS technique is based upon the wavelength dependent absorption of light over a specified light path.  
118 The miniDOAS instruments offer greater portability and a lower cost relative to prior DOAS instruments  
119 (Volten et al., 2012). The broadband and narrowband extinction of UV-light (=absorption + scattering) is  
120 measured across the light path, and the concentration of different trace gases is determined by their respective  
121 absorption spectra (details in Sintermann et al., 2016). In the wavelength range used by the miniDOAS (204 –  
122 230nm), narrowband-absorption is seen by NH<sub>3</sub>, sulphur dioxide (SO<sub>2</sub>), and nitrogen oxide (NO), while other  
123 | absorbers with broader absorption features are eliminated by high-pass-filtering. The systems were calibrated  
124 ~~prior to the field experiment~~ using a flow-cell in the miniDOAS light path with a high-concentration NH<sub>3</sub> gas  
125 standard; in addition, the cell's outlet-flow was checked by wet chemical impinger samples (two in a row) and  
126 photometric NH<sub>3</sub> determination. ~~Details are presented by Sintermann et al., (2016).~~ Reference spectra ( $I_{ref}$ , see  
127 | Sintermann et al., 2016) were determined for each instrument ~~during an inter-comparison phase~~ at the field site  
128 one week prior to the grazing experiment, where the three miniDOAS systems were configured to measure in  
129 parallel (measuring concentrations across the same open-path). In order to provide the absolute concentration



130 reference ( $c_{\text{ref}}$ , see Sintermann et al., 2016) for the miniDOAS, a transect of three sets of ALPHA passive  
131 sampler triplicates (Tang et al., 2001) were placed along the path length, giving a time-integrated  $c_{\text{ref}}$   
132 measurement. The miniDOAS inter-comparison showed close agreement in the concentration levels between the  
133 three systems, where the coefficient of variation was 3.4% (unpublished data). ~~A revision~~ The random  
134 uncertainty of the miniDOAS measurements was determined to be 1.4% of the concentration levels, however  
135 not lower than  $0.2 \mu\text{g m}^{-2} \text{s}^{-1}$  (Sintermann et al., 2016). Since the initial miniDOAS publication (Sintermann et  
136 al., 2016) the calibration procedure applied by Sintermann et al. (2016) led to an increase in the slope by 16%,  
137 due has been revised to correct a gas standard correction error in the conversion from ppm to  $\mu\text{g m}^{-3}$ . The  
138 corrected measurements presented in this study are a factor of 1.16 higher relative to the  $\text{NH}_3$  concentrations  
139 presented by Sintermann et al., (2016).

140 To measure horizontal concentration gradients across the field, three miniDOAS instruments were placed  
141 strategically (based on the forecasted wind direction) at field boundaries at heights 1.4m above the ground, on  
142 stands drilled into the ground for stability. Retro-reflectors were set 37m away from each light source at the  
143 same height. A sensor placed upwind of the field would measure the background concentration ( $C_b$ ), which can  
144 be subtracted from the downwind concentration measurements ( $C$ ) to determine the horizontal concentration  
145 gradient or excess in concentration caused by emissions ( $\Delta C$ ). The miniDOAS concentration measurements  
146 were recorded at 1-minute averaging intervals, and later averaged to 30 minute intervals for analysis.

### 147 2.3 Micrometeorological measurements

148 A three-dimensional ultrasonic anemometer (Gill Windmaster, Gill Instruments Limited, Lymington, UK) was  
149 mounted on an instrument tower at 1.5m height above the ground within a fenced-off section in the centre of the  
150 field. ~~The~~ The sonic anemometer measured the three orthogonal wind components ( $u, v, w$ ,  $\text{m s}^{-1}$ ) ~~and at a~~  
151 frequency of 20 Hz, along with a fast temperature measurement ~~were logged at a frequency of 20 Hz.~~ Later the  
152 eddy covariance measurements were processed over 30 minute averages, and the friction velocity ( $u^*$ ,  $\text{m s}^{-1}$ ),  
153 surface roughness ( $z_0$ , cm), Monin-Obukhov length ( $L$ , m), standard deviations of the rotated wind components  
154 ( $\sigma_u, \sigma_v, \sigma_w$ ), and resultant horizontal wind speed ( $u$ ,  $\text{m s}^{-1}$ ) and wind direction ( $wd$ ) were computed. Correction  
155 factors were applied to fix a 'bug' implicit within the Gill Windmaster instrument, as recommended by the  
156 manufacturer (Gill Instruments, 2016). The applied correction was a multiplication factor of 1.166 applied to  
157 positive vertical  $w$  wind axis measurements, and a factor of 1.289 applied to negative  $w$  wind axis  
158 measurements.

159 Mounted on the instrument tower at 2m height was a HMP45C sensor (Campbell Scientific, Loughborough,  
160 UK) which provided temperature ( $T$ , °C) and relative humidity ( $RH$ , %) measurements. Leaf wetness ( $LW$ , %  
161 time wet) at canopy level was measured by a specialised conductivity sensor (Campbell Scientific,  
162 Loughborough, UK) placed 10 cm above the ground.

### 163 2.4 Dispersion modelling

164 The ~~backward Lagrangian Stochastic (bLS)~~ type dispersion model is frequently applied for the computation of  
165 the inverse dispersion method (Flesch et al., 2004). Driven by measurements of the prevailing wind conditions,  
166 and with knowledge of the rise in concentration above background ( $\Delta C$ ) caused by an emitting source, the  
167 model can be applied to estimate the emission rate that best fits the measured concentration data. The measured

wind statistics ( $\sigma_u, \sigma_v, \sigma_w$ ), atmospheric frictional velocity ( $u^*$ ), wind direction ( $wd$ ) and surface roughness ( $z_0$ ) describe the windflow characteristics, surface drag and buoyancy which enables the dispersion model to relate the downwind concentration fields to emissions from the source area. Within the horizontally homogenous surface layer (height  $z < 100\text{m}$ , but above canopy level), the wind and turbulence measurements should be representative of the atmosphere over the entire site, thus the sonic anemometer location is not critical. A condition of the bLS method states that the terrain should be tolerably homogenous (Flesch et al., 2004), this criterion was met by the study site which consisted entirely of short grass (10-20cm canopy height).

During bLS simulation the trajectories of thousands of fluid particles are calculated backwards in time from a reference point (concentration receptor) under the prevailing wind conditions. The locations where the trajectories intersect the ground (“touchdowns”) and proportion of these which fall within the source area ( $N_{source}$ ) are used to calculate ( $\Delta C/Q$ ), along with the associated vertical velocity ( $w_0$ ) of each touchdown (for details see Flesch et al., 1995; 2004).

The bLS-R model (Häni, 2016), is an inverse dispersion model that is based upon the backward Lagrangian stochastic dispersion theory described by Flesch et al., (1995; 2004); however bLS-R has an additional function which computes the effect of dry deposition on gas concentrations. The bLS-R package provides functions to set up and execute the model within the R statistical software (R Core Team, 2015). ~~The~~ Driven by the wind and turbulence inputs, for each time interval the model calculates the dispersion coefficient  $D$  ( $\text{s m}^{-1}$ ), used specific to derive the flux emitted from the source–receptor geometry. The emission flux ( $Q$ ,  $\mu\text{g m}^{-2} \text{s}^{-1}$ ), by may then be calculated from the measured rise in concentration above background ( $\Delta C$ ) (Eq. 1).

$$Q = (\Delta C) * D^{-1} \quad (1)$$

where  $D$  is retrieved by the model from the number of source area interactions ( $N_{source}$ ) and the thousands of trajectories ( $N$ ) released backwards in time from the receptor locations (Eq. 22), and the vertical “touchdown velocities” at impact ( $w_0$ ) (for details see Flesch et al., 2004).

$$D = \frac{1}{N} \sum N_{source} \left| \frac{2}{w_0} \right| \quad (2)$$

The following input data were applied in the bLS-R model as 30 minute averages: wind direction, frictional velocity ( $u^*$ ) the standard deviations of the rotated wind vector components ( $\sigma_u, \sigma_v, \sigma_w$ ), and surface roughness ( $z_0$ ). The spatial dimensions of the grazed field source area and the miniDOAS receptors were also specified.

Independent concentration measurements and emission estimates were derived using the two downwind miniDOAS receptors (S1 and S3), which are compared throughout the paper, e.g. CS1, CS3 and QS1, QS3. All concentrations and fluxes are expressed in units of  $\text{NH}_3$ , e.g.  $\mu\text{g NH}_3 \text{ m}^{-3}$  and  $\mu\text{g NH}_3 \text{ m}^{-2} \text{ s}^{-1}$ .

## 2.5 Data filtering

The miniDOAS  $\text{NH}_3$  measurements were filtered to remove periods of high uncertainty, indicated by the standard error (SE) of the measurements. This filter only affected the S1 miniDOAS sensor, which was not fitted with an automatic alignment system to correct minor shifts in the light path between lamp and reflector. After applying this filter 92 out of 430 half hourly measurements were removed from the Period 2 S1 measurements (Period 1 measurements were unaffected).

205 Previous studies (Flesch et al., 2004; Harper et al., 2011) have applied  $u^*$  and Monin-Obukhov length ( $L$ )  
206 filtering to remove emission estimates that do not meet given criteria ( $u^* > 0.15 \text{ ms}^{-1}$  and  $L > 10\text{m}$ ). These  
207 criteria were established on the basis of an observed reduction in the accuracy of model predictions as  $u^*$  and  $L$   
208 decrease (e.g., Flesch et al., 2004; Gao et al., 2009). However, filtering out periods with low wind speeds and  
209 unstable stratification can be detrimental to emission estimates, often creating a bias to characterise certain  
210 sources under specific daytime or night-time conditions, whilst ignoring potentially valuable data that do not  
211 meet the criteria. This is a major limitation as we calculate average emissions from grazing cattle, where strong  
212 diurnal cycling is expected to occur (e.g. Laubach et al., 2013a). Flesch et al., (2014) developed alternate criteria  
213 for bLS data filtering, finding that (for their particular experiment) the  $u^*$  threshold could be reduced to  $0.05 \text{ m}$   
214  $\text{s}^{-1}$ , and after finding no improvement after imposing a stability ( $L$ ) filter, introduced a supplementary vertical  
215 temperature gradient filter.

216 A filtering procedure was developed after assessing the standard error (SE) of emission estimates ( $\sigma_{Q/Q}$ ), which  
217 describes period-to-period fidelity and identifies “spiking” in model predictions caused by unsuitable input  
218 conditions, which do not confirm to an underlying assumption of a horizontally homogenous surface layer  
219 (Flesch et al., 2014). It was found that a  $u^*$  threshold of  $0.1 \text{ m s}^{-1}$  was sufficient to remove the significant  
220 outliers, while retaining acceptable data coverage, although this filter was at times limiting for nocturnal (low  
221 wind) periods. A wind direction filter was applied to remove periods where miniDOAS sensors S1 and S3 were  
222 not downwind of the field area. This filter only affected sensor S3 during Period 2, where estimates were  
223 ignored if  $wd > 30$  &  $wd < 270$ .

## 224 2.6 Modelling of dry deposition within the source area

225 Downwind from a source of  $\text{NH}_3$ , local recapture will remove a certain fraction of emitted  $\text{NH}_3$  from the air.  
226 Therefore, the measured rise in concentration above background ( $\Delta C$ ) is a function of the source emission rate,  
227 atmospheric dispersion, and the fraction that has been deposited. Within a field being grazed by dairy cattle,  
228 emissions of  $\text{NH}_3$  are expected from urine and dung patches, while deposition will occur to clean surfaces  
229 within and beyond the field. ~~Therefore, as~~ we apply the bLS method to estimate emissions from the  
230 ~~measured~~ concentration gradient across the field ( $\Delta C$ ), we calculate the “net” flux constituting  
231 emissions from the field minus the fraction that has been deposited. However, if dry deposition is simulated in  
232 the dispersion model the lost fraction of emissions due to deposition can be quantified, providing an estimate for  
233 the “gross” emissions from excretions during grazing.

234 The bLS-R model has a post-processing routine to ~~take into account~~ simulate the effect of the dry deposition of  
235  $\text{NH}_3$  on flux predictions. The exchange or deposition velocity ( $v_d$ ,  $\text{cm s}^{-1}$ ) is based upon a uni-directional  
236 resistance model approach, defined as the inverse of a sum of a series of resistances to deposition (Eq. 3, left  
237 side) (Wesley and Hicks, 2000).

$$238 \quad v_d = \frac{1}{R_a + R_b + R_c} = \frac{-F}{C} \quad (3)$$

239 where  $R_a$  is the aerodynamic resistance to transfer through the turbulent surface layer for a certain reference  
240 height,  $R_b$  is the boundary layer resistance associated with the viscous quasi-laminar sublayer adjacent to the  
241 deposited surface, and  $R_c$  is the canopy resistance representing the combined surface resistance accounting for

242 stomatal and non-stomatal pathways to deposition (Flechard et al., 2013). It should be noted that  $R_a$  is implicit  
243 within the bLS-R calculations and does not need to be input to the model as a variable.

244 The uni-directional resistance model treatment is based upon strongly simplified assumptions regarding the  
245 near-ground  $\text{NH}_3$  concentrations and respective  $\text{NH}_3$  deposition flux, since the exchange of  $\text{NH}_3$  to ecosystems  
246 is bi-directional, involving many complex processes (Kruit et al., 2010; Fowler et al., 2009; Flechard et al.,  
247 2013).

248 The resistances to deposition  $R_a$  and  $R_b$  can be calculated using ultrasonic anemometer measurements and well-  
249 established models (Asman, 1998), while  $R_c$  is a composite term representing numerous physical barriers to  
250 deposition at the surface. To obtain local, field-scale estimates of  $R_c$ , ~~Two~~ COTAG systems (conditional  
251 time-averaged gradient systems, Famulari et al., 2010) were operated at the centre of the grazed field for 1.5  
252 years, allowing  $R_c$  to be estimated from calculations of  $R_a$  and  $R_b$  and time-integrated measurements of  $\text{NH}_3$   
253 concentration ( $C$ ), flux ( $-F$ ) and  $v_d$  (Eq. 3). The COTAG measurements were filtered to remove grazing  
254 periods and periods up to two weeks after grazing had ended, to ensure ‘clean’ background conditions. Clear  
255 correlation was then observed between the time-integrated  $R_c$  estimates with the variables  $T$  ( $^{\circ}\text{C}$ ) and  $RH$  (%),  
256 thus a double exponential equation was parameterised as follows to fit the data (Eq. 4, Figure 2), with similar  
257 form to Flechard et al., (2010):

$$258 \quad R_c = R_{c, \min} \times \exp^{\alpha \times (100 - RH)} \times \exp^{\beta \times Abs(T)} \quad (4)$$

259 A curve fitting procedure provided estimates of the parameters  $\alpha$ ,  $\beta$  and  $R_{c, \min}$  as 0.013 and 0.015  $^{\circ}\text{C}^{-1}$  and 10 s  
260  $\text{m}^{-1}$ , respectively.

261 The deposition component of bLS-R operates on the assumption that the whole grazed field is acting as a  
262 homogenous surface for deposition, however in reality urine and dung patches on the field are obviously  
263 hotspots of emissions, and not  $\text{NH}_3$  sinks. The ratio of ‘clean canopy’ where deposition may occur to ‘soiled  
264 canopy’ is not known, thus it is difficult to provide a true emission estimate including the effect of deposition.  
265 We can expect that the emission estimate without deposition ( $Q$ ) represents a ‘net’ emission rate from the field,  
266 while if we assume that the whole field behaves as homogenous sink, the emission rate including deposition will  
267 represent an upper limit of the gross emission estimate. The actual emission rate for a soiled field can be  
268 expected to fall somewhere in between the net and upper gross estimates.

269 A means of addressing this issue with the heterogeneous canopy surface may be found in reviewing the  $R_c$   
270 timeseries derived from the time-integrated COTAG concentration and flux measurements on the field, as  $v_d$   
271 acts on the local vertical concentration gradient between surface and reference height, i.e. the flux is  
272 concentration-gradient driven. At certain periods over the course of the year cattle were brought onto the field  
273 for grazing, and shortly after the grazing periods had ended the  $\text{NH}_3$  flux would return back to the negative  
274 (deposition), and therefore  $R_c$  could be calculated. Averaging all ~~of~~ the COTAG  $R_c$  calculations within one  
275 month following each grazing period gives an  $R_c$  value of 260  $\text{s m}^{-1}$ , and comparing this value with the average  
276  $R_c$  where there had been no grazing on the field for at least one month (130  $\text{s m}^{-1}$ ). ~~Therefore~~  
277 ~~fertilisation~~ However, there was considerable scatter in the data, with standard deviations of 200  $\text{s m}^{-1}$  and 40  $\text{s m}^{-1}$   
278 for the post-grazing and “clean” periods respectively. Fertilisation of the field surface through grazing appears  
279 to have caused an increase in  $R_c$  of 130  $\text{s m}^{-1}$ . This measured increase caused by excreted N to the field surface  
280 has been applied as an offset to the modelled  $R_c$  estimated by Eq. 4, and has been input to bLS-R. The bLS  
281 emission estimates without including deposition are referred to as  $Q$ , while the estimates including deposition

282 and the  $R_c$  offset are referred to as  $Q_{dep}$ . Emission estimates including deposition but without the  $R_c$  offset are  
283 referred to as  $Q_{depmax}$ .

## 284 2.7 N excretion model

285 To contribute towards an emission factor for cattle grazing and to compare with literature values, it was  
286 necessary to express the emission estimates as a fraction of excreted N or urine-N. A nitrogen excretion model  
287 based on the Swiss feeding recommendations for dairy cows (Menzi et al., 2015; Muenger personal  
288 communication) was applied to quantify the total N and urine-N excreted to the field during both grazing  
289 periods, from the following set of inputs: (1) milk yield, (2) animal numbers, average weight and date after  
290 calving, (3) the net energy for lactation (NEL) and crude protein (CP) content of the grass, (4) the number of  
291 animals grazed and the duration of grazing on the experimental plot. The excretions per day were calculated as  
292 consumption minus retention in milk and animal growth. The share of N excreted in faeces and urine was  
293 calculated using regressions of fecal N digestibility derived from N balance studies (Bracher et al., 2011;  
294 2012).

## 295 3. Results

### 296 3.1 Period 1 (18-20/05): grazing on SW paddock only

#### 297 3.1.1 Concentration measurements

298 The wind direction during Period 1 was consistently W-WSW (Figure 3). Therefore, DOAS S2 was located  
299 upwind of the grazed SW paddock while S1 and S3 were situated downwind to the eastern and northeastern  
300 boundaries of the field respectively. Concentrations across the S2 path length would be expected to be low and  
301 near background, except during periods of very low wind speed, while any rise in concentration measured by S1  
302 and S3 above S2 would show the influence of emissions from the field.

303 The upwind S2 concentration measurements reveal background concentrations of 2-3  $\mu\text{g m}^{-3}$  during times of  
304 steady W/SW winds, increasing slightly when wind speed was low. Concentration polar plots (Figure 3) show  
305 the average concentrations measured as a function of wind speed and direction, where the influence of emissions  
306 from the grazed field is illustrated by the increase in measured concentrations at downwind receptors S1 and S3  
307 relative to S2 ( $C_b$ ).

308 Power failure led to a partial loss of measurements from miniDOAS S2, which are required to specify  $C_b$  for  
309 estimating emissions through bLS modelling. A significant linear regression was found between the measured  
310 background S2 concentration and wind speed ( $u$ ,  $\text{m s}^{-1}$ ), temperature ( $T$ ,  $^{\circ}\text{C}$ ) and relative humidity ( $RH$ , %):

$$311 \quad C_b = 4.26 - 0.59u + 0.06T - 0.017RH, r^2 = 0.5 \quad (5)$$

312 The wind direction remained consistent after the S2 power failed on 19/05, therefore the empirical relationship  
313 (Eq. 5) was found to be suitable and was applied to estimate and extend S2 concentrations, as a proxy for  $C_b$ .  
314 The predicted S2 concentrations follow the measured S2 concentrations closely until the point of data loss on  
315 19/05 (Figure 4, top panel). This lends confidence to the rest of the  $C_b$  predictions used to fill the gap in the  
316 measurements, even though there is increased uncertainty associated with the last 15 hours of emission  
317 estimates calculated from the predicted  $C_b$ , relative to periods where  $C_b$  was measured by the S2 sensor.

### 318 3.1.2 Field-scale emissions estimates

319 Overall there is very good agreement between the emission calculations from both downwind concentration  
320 datasets. The average emission rate calculated by bLS-R for the S3 measurements ( $QS3$ ) is  $0.29 \mu\text{g m}^{-2} \text{s}^{-1}$ ,  
321 while the  $QS1$  average is  $0.27 \mu\text{g m}^{-2} \text{s}^{-1}$ . The modelled emission of  $\text{NH}_3$  is low (generally below  $0.2 \mu\text{g m}^{-2} \text{s}^{-1}$ )  
322 during the first 24 hours, as the measured concentration gradient across the field was less than  $1 \mu\text{g m}^{-3}$ . As the  
323 cattle were introduced to the field on the first morning (18/05) it likely took some time for  $\text{NH}_3$  to ‘build up’  
324 from hydrolysis of excreted urea before significant emissions occurred. Downwind concentrations ( $CS1$  and  
325  $CS3$ ) peaked during the next day (19/05), with peak emissions occurring at midday when there was a  $5\text{-}6 \mu\text{g m}^{-3}$   
326 horizontal concentration gradient ( $\Delta C$ ) measured between the upwind and downwind receptors. The peak  
327 emission rate at this time was around  $1.1 \mu\text{g m}^{-2} \text{s}^{-1}$  for both downwind receptors. A decrease in the measured  
328 downwind concentrations occurred at 15:00, and an associated decrease in emissions is logically estimated for  
329 this time period. The decline in emissions follows 4.4 mm of rain during the day of 19/08, where the rainfall  
330 intensity peaked shortly after midday. In addition, the cattle were removed from the field at 15:00; therefore the  
331 suspension of excretions to the field and the wet conditions are most likely the dominant factors driving the  
332 declining emissions. The  $LW$  sensor indicated that the canopy was wet (conductivity reading above baseline) for  
333 84% of Period 1 (Table 2).

334 Coinciding with the daytime peak in emissions and downwind concentrations were peaks in  $T$  and  $u$ , while  $RH$   
335 reached a minimum (Figure 4). During the night emissions decreased to near 0, where  $RH$  reaches a maximum  
336 and  $T$  and  $u$  reach a minimum. The average  $Q_{dep}$  gross emission estimates are greater than the  $Q$  net emission  
337 estimates by 13-16%.

## 338 3.2 Period 2 (20-29/05): grazing on whole field

### 339 3.2.1 Concentration measurements

340 Concentration measurements during Period 2 (20-29/05) revealed considerable differences between downwind  
341 receptors, where the average  $CS1$  at the center of the field was much greater than the average  $CS3$  at the SE  
342 corner (Figure 5), with period averages of  $5.6 \mu\text{g m}^{-3}$  and  $3.9 \mu\text{g m}^{-3}$ , respectively. This may be partially  
343 explained by the location of the receptors relative to the grazed field under the prevailing wind conditions.  
344 Sensor S1 was located in the center of the field, with an upwind fetch of grazed field across a wider band of  
345 wind directions. Sensor S3 on the other hand is located at the SE field boundary, and was more limited as a  
346 receptor for emissions under the prevailing northerly wind conditions. However, during NW wind directions  
347 where all sensors in-line across a diagonal fetch of the field one would expect the S3 sensor to be measuring  
348 similar or higher concentrations relative to S1 at the center (assuming homogenous emissions across the field),  
349 which is not the case. It is also important to note that the grazing density was about 50% lower during Period 2  
350 as the field was much larger.

351 Power failure led to significant data gaps from the S2 sensor and hence a loss of  $C_b$  measurements (Figure 6).

352 To fill the gaps a linear regression was applied between the measured S2 concentration and ~~temperature ( $T$ ),~~  
353 ~~wind speed ( $u$ ), and relative humidity ( $RH$ ), however.~~ However, there was considerable scatter in the data and  
354 the  $C_b$  prediction was much more uncertain than during Period 1.

$$355 \quad C_b = 2.5 - 0.1u + 0.01T - 0.02RH, r^2 = 0.1 \quad (6)$$

### 3.2.2 Field-scale emissions estimates

The average net emission rate ( $Q$ ) from the grazed field estimated using the S1 measurements was  $0.27 \mu\text{g m}^{-2} \text{s}^{-1}$  while much lower emissions were estimated from the S3 measurements ( $0.12 \mu\text{g m}^{-2} \text{s}^{-1}$ ). Both estimates show a generally diurnal trend of peak emissions during the afternoon, similar to the trend observed during Period 1. However, there are gaps in  $QS1$  and  $QS3$  overnight due to data filtering as  $u^*$  drops below the defined threshold ( $0.1 \text{ m s}^{-1}$ ). Peak emissions occurred on 22/05 when the maximum concentration difference between upwind and downwind receptors was measured. Grazing of the field ended and the cattle left the field at 15:00 GMT on 23/05. After this point a generally decreasing trend in emissions is derived from the decreasing concentrations measured by S1 and S3. There is greater uncertainty attributed to the periods without active  $C_b$  measurements marked on Figure 6.

Emission estimates from the bLS-R model were initially made on the assumption that emissions from the grazed field are spread equally (thus randomly) across a homogeneous field. However a herd of cattle can be expected to move and disperse across the field in a generally non – random way, grouping together as they graze across the field rather than acting individually. Systematic effects of uneven cattle distribution within grazed pastures have been reported previously, impacting on bLS-derived mean gaseous emissions from grazing cattle (Laubach et al., 2013b). Our measurements during Period 2 certainly support spatial heterogeneity in emissions, with higher concentrations at the centre of the field (CS1) than at the SE corner (CS3) during periods wherein which the wind direction was from the NW. Had the emissions from the field been spatially homogenous, as these emissions are taken up by the atmosphere and dispersed, an increase in  $\text{NH}_3$  concentration would have been measured with distance downwind across the NW - SE transect of the field, causing higher concentrations at S3 compared to S1.

A second set of emission estimates (Figure 6 Panel 3) were produced after optimising the emission rates from 4 separate areas (A, B, C & D, Figure 1) within the field to reproduce the observed concentrations at S1 and S3 on each measurement day. An excellent fit between  $QS1$  and  $QS3$  was achieved after running a numerical solver to minimise the squared error ( $e^2$ ) between them. The coefficients given in Table 1 are the result of the solver, describing the spatial changes in relative emission strength over time. The solver was executed with the following conditions: (1) the sum of the area coefficients must equal 1; and (2) no area coefficient can be below 0.075. The minimum value for any area coefficient ( $AC_{min}$ ) is a parameter which describes the heterogeneity of emissions, where in this case it was assumed that each source area must contribute at least 30% of the original (homogenous) value.

Henceforth the initial emission estimates calculated without applying emission area coefficients are referred to as Scenario 1 estimates, while the calculations involving heterogeneous emission area coefficients are referred to as Scenario 2 estimates. It is important to note that there can be more than one combination of coefficients to reconcile the  $QS1$  and  $QS3$  estimates, thus these coefficients should not be taken as definite emission strengths for each area of the field. However, they do offer a rough guide to which sections had greater emissions relative to the others, and confirm that emissions from the field were certainly not homogeneous over the course of the grazing period. The large difference in Scenario 1  $QS1$  and  $QS3$  estimates may therefore be attributed to strong emissions in areas A and D, relative to C and B (Figure 1, Table 1), which explains the high measured concentrations at sensor S1 relative to S3. Emission area D represents the SW field which was grazed during Period 1, thus high emissions from this area may have been a legacy effect left by continuing emissions from

396 cattle excretions during Period 1. Emission area D also contained a water trough which was only 15-20m away  
397 from the S1 receptor, where cattle grouping was observed. Due to the combined effects of prior grazing within  
398 the SW field and grouping around the water trough, we can expect enhanced emissions within area D. The  
399 Scenario 2 (optimised)  $QS1$  and  $QS3$  estimates are similar ( $0.19$  and  $0.16 \mu\text{g m}^{-2} \text{s}^{-1}$  respectively), and are  
400 believed to give a more realistic estimate of the true field-scale emission rates after accounting for spatial  
401 complexity. The data coverage for  $QS3$  (64%) is greater than the  $QS1$  data coverage (59%), hence some  
402 differences between  $QS1$  and  $QS3$  can be expected even with perfect agreement. The  $Q$  estimates can be  
403 regarded as net emission rates for the grazed field, made without consideration of deposition to clean patches  
404 within the source area. The  $Q_{dep}$  estimates including the effect of deposition are 16% higher ( $0.22$  and  $0.19 \mu\text{g}$   
405  $\text{m}^{-2} \text{s}^{-1}$  for the Scenario 2 S1 and S3 estimates respectively).

### 406 3.3 Derived emission factors

407 Grazing Period 1 took place within a SW section of the field with a smaller area ( $5600 \text{ m}^2$ ) than the whole field  
408 opened up for grazing Period 2 ( $19800 \text{ m}^2$ ). Although there were fewer cattle grazing during Period 1 (25) the  
409 grazing density was twice as high relative to Period 2. Therefore, the higher grazing density during Period 1 is  
410 consistent with the stronger emission estimates per unit area (Table 2). Emission factors (EFs) are given in  
411 Table 3 for Periods 1 and 2. For both measurement periods, the S3 sensor had greater data coverage than the S1  
412 sensor. Therefore, the S3 emission estimates are more representative and are selected to derive EFs. Both  
413 grazing periods have produced similar emission factors of the order of  $6\text{-}7 \text{ g NH}_3 \text{ cow}^{-1} \text{ d}^{-1}$ , though there are  
414 considerable differences between the two periods in terms of weather conditions and grazing timeline. Period 1  
415 was shorter in length, and was characterised by steady SW/W winds, lower temperatures and wetter conditions  
416 relative to Period 2 (Table 2). Therefore, the lower temperatures and wetter conditions likely limited emissions  
417 (e.g. Flechard et al., 1999; Laubach et al., 2012; Möring et al., 2016).

418 The duration of Period 1 was too short to fully capture tailing emissions, while excretions to the field during  
419 Period 1 will have continued to emit  $\text{NH}_3$  during Period 2. Flux estimates are continued for 6 days after the  
420 cattle had left the field during Period 2, capturing residual emissions after grazing. The combined influences of  
421 weather conditions and experimental design and duration may therefore explain why a smaller fraction of  
422 excreted N and urine-N was emitted as  $\text{NH}_3$  during Period 1 relative to Period 2. The EFs derived from Period 2  
423 fluxes may for these reasons be considered to be more representative of the total emissions from grazing, where  
424 emissions are estimated to be  $6$  and  $7 \text{ g NH}_3 \text{ cow}^{-1} \text{ d}^{-1}$ , and  $9$  and  $10\%$  excreted urine-N emitted as  $\text{NH}_3$  for the  $Q$   
425 and  $Q_{dep}$  scenarios respectively. However, the greater uncertainty in Period 2 associated with missing  $C_b$   
426 measurements and heterogeneous emission patterns should be considered.

## 427 4. Discussion

### 428 4.1 Experimental design

429 Previous experiments to deduce surface-air fluxes by the bLS method have deployed sufficient measurement  
430 systems so that the problem to determine  $C$  and  $C_b$  was mathematically over-determined, and the experiment  
431 was not dependent on a specific range of wind directions (e.g. Flesch et al., 2014). The configuration of the  
432 three miniDOAS sensors and the grazed field during Period 2 led to certain wind directions being unsuitable for



433 emission estimates, while additional miniDOAS sensors placed at field boundaries would have been beneficial.  
434 However, the configuration of the miniDOAS sensors was optimised by using the weather forecast to predict the  
435 wind direction prior to the grazing experiment and placing the miniDOAS sensors accordingly.  
436 It was originally hypothesised that the model could treat the field area as a spatially homogenous source, where  
437 emission estimates would show insensitivity to cattle grouping and excretion patterns within the field. This  
438 assumption seemed valid for the Period 1 emission estimates, where very good agreement was achieved in  $C$   
439 and  $Q$  between the downwind receptors. The SW field grazed during Period 1 was smaller than the whole field  
440 grazed during Period 2, and the wind direction was more consistent. This allowed the downwind and upwind  
441 receptors to capture the inflow and outflow concentrations and produce reliable emission estimates, while the  
442 grazing density was higher. During Period 2 the field was larger and the grazing density was 50% lower, which  
443 led to some spatial and temporal emission ‘hotspots’ caused by cattle grouping and/or excretions within certain  
444 areas, such as around the water trough. The S1 sensor was located very close to a ~~particular~~ ‘hotspot’ of  
445 emissions at the centre and SW section of the field, while the S3 sensor was located next to an area (SE corner)  
446 which appears to have seen relatively little emissions. Because of this the model could not treat the field as a  
447 homogenous source area and reconcile emission estimates between downwind receptors, and source-area  
448 differentiation (Table 1) was required. ~~Therefore~~ Clearly, there is a limitation in the application of the standard  
449 bLS method to estimate emissions from area sources which may not be treated as homogenous, such as pastures  
450 with a low grazing density. However, as the Period 2/Scenario 2 emission estimates demonstrate it may also be  
451 possible to account for this heterogeneity if more than one downwind concentration receptor is used and they are  
452 suitably located. Insensitivity to heterogeneous emissions has been demonstrated if concentration measurements  
453 are made at least twice as far downwind as the maximum distance between potential sources (Flesch et al.,  
454 2005). Therefore, had the miniDOAS sensors been placed differently to satisfy this criterion it is possible that no  
455 source area optimisation would have been necessary to reconcile bLS emission estimates. ~~However~~ On the other  
456 hand, as emissions from excretions to the grazed pasture were relatively weak, at a greater distance downwind  
457 from the field the concentration rise above background may not be significant enough to evaluate the emissions.  
458 Felber et al., (2015) applied corralling of grazing cattle into paddocks over a rotational grazing cycle to increase  
459 grazing density, and placed GPS trackers on individual cattle to attribute eddy covariance methane fluxes using  
460 a footprint model. The Period 1 emission estimates demonstrate that a smaller paddock and higher grazing  
461 density can be a solution to the heterogeneous emissions problem, however  $\text{NH}_3$  emissions from grazing cattle  
462 arise from excretions to the field surface and are not enteric, hence GPS trackers on cattle may not track the  $\text{NH}_3$   
463 emissions directly as they do for methane. In order to accurately attribute fluxes from grazed pastures there is  
464 call to develop a method to track excretions spatially and temporally across a grazed field, potentially using  
465 visual observations or cameras and animal detection software. We did carry out visual observations of urination  
466 events during Period 1 (day time only), which described a fairly homogenous distribution (data not shown, Andi  
467 MÓring, personal communication). ~~However~~ Unfortunately, observations ~~were~~ could not be carried out during  
468 Period 2.

## 469 4.2 Uncertainty in field-scale emission estimates

### 470 4.2.1 Uncertainty in miniDOAS concentration measurements and dispersion model

471 The instrumental uncertainty associated with the miniDOAS concentration measurements was evaluated during  
472 the initial inter-comparison phase, where the systems were configured to measure in parallel. Very good  
473 agreement was observed between the analysers, with a slope of one and an intercept close to zero. Deviations  
474 between the S1, S2 and S3 analysers were minor, and the coefficient of variation between them was determined  
475 to be 3.4% (unpublished data). Sintermann et al. (2016) have described this inter-comparison phase and the  
476 miniDOAS performance in detail, however the authors compare only the miniDOAS sensors S2 and S3 as these  
477 sensors were fitted with all of the updated Swiss miniDOAS instrumental features discussed within that study.

478 Since the input data had been filtered to remove conditions which do not meet the established criteria ( $u * < 0.1$   
479  $m s^{-1}$ ), and instrumental uncertainty associated with the concentration measurements is very low, the principal  
480 uncertainties are associated with the modelled results, principally the input variables which could not be  
481 measured directly, such as  $R_c$ , and the predicted background concentration  $C_b$  used for gap-filling.

482 The bLS dispersion model theory has been well validated in past experiments (e.g. Flesch et al., 2004; McGinn  
483 et al. 2009), however we can assume a general overall uncertainty based on evaluated performance by an  
484 ensemble of published trace gas release experiments. A review of 24 bLS tracer release assessments (Häni et al.,  
485 2016) found that the uncertainty is generally between 10 and 20% for the bLS method.

### 486 4.2.2 Uncertainty in background concentration

487 The background concentration ( $C_b$ ) had to be predicted to “fill in” the gaps in the  $C_b$  measurements upwind of  
488 the field measured by miniDOAS sensor S2. Multiple regression equations (Eq. 5; 6) were based on previous  
489 observations that background  $NH_3$  is dependent on wind speed, temperature and relative humidity (Flechard and  
490 Fowler, 1998), but nonetheless error is introduced due to differences between the predicted  $C_b$  and the actual  $C_b$ .

491 The mean absolute error (MAE) between the measured and predicted  $C_b$  for Periods 1 and 2 have been applied  
492 to offset to the predicted  $C_b$  timeseries input to the model, to determine the limits (upper and lower) of emission  
493 estimates caused by this uncertainty. The MAE between the observed and predicted background concentrations  
494 during Period 1 was  $0.33 \mu g m^{-3}$ , while the percentage of data coverage (observed  $C_b$  measurements) was 67%.  
495 Measurement Period 2 had a greater MAE between observed and predicted  $C_b$  ( $0.56 \mu g m^{-3}$ ) (Table 4), as the  
496 multiple regression equation used to fill ( $C_b$ ) measurement gaps did not give very accurate predictions (Eq. 6).  
497 Furthermore, the upwind sensor S2 was only active during 44% of the measurement period; therefore the Period  
498 2 emission estimates are more sensitive to this uncertainty. The % change in  $Q_{dep}$  to predicted  $C_b \pm MAE$  was  
499 much greater during Period 2 ( $\pm 31\%$ ) than Period 1 ( $\pm 5\%$ ).

### 500 4.2.3 Uncertainty in local dry deposition of field-emitted $NH_3$

501 The inclusion of dry deposition within the bLS-R model is intended to simulate the deposition of  $NH_3$  to the  
502 surface of ‘clean’ grass patches within the grazed field. This process is described by a resistance model, and  
503 while the  $R_a$  and  $R_b$  components may be derived directly from eddy covariance measurements, as well as well-  
504 established models, the  $R_c$  component is empirical. In this case, the empirical  $R_c$  model (Eq. 4) was derived  
505 from a curve fitting exercise of time-integrated COTAG flux measurement to meteorological variables  $T$  and

506 *RH*. The  $R_c$  model is based on a long (1.5 years) series of measurements taken from the field (deposition periods  
507 only), while the effect of soiled grass areas on  $R_c$  during grazing is also approximated using the  $130 \text{ s m}^{-1} R_c$   
508 offset within the  $Q_{dep}$  scenario. It is conceivable that there is significant error (up to 50%) in estimating  $R_c$  by  
509 this method. The sensitivity of the bLS-R model to potential uncertainty within the  $R_c$  estimates has been  
510 evaluated, where the  $R_c$  timeseries has been varied by factors of plus and minus 50%. The results of this  
511 sensitivity test are given in Table 4. The % change in  $Q_{dep}$  after varying  $R_c$  by  $\pm 50\%$  was  $-4\%$  and  $+12\%$  for  
512 Period 1 and  $\pm 5\%$  for Period 2.

513 While impact of this uncertainty on the absolute value for  $Q_{dep}$  is not very large, the change in  $Q_{dep}$  relative to  
514  $Q$  is significant. The Period 2  $Q_{dep}$  uncertainty due to predicted  $R_c$  is  $\pm 5\%$ ; therefore including deposition in the  
515 model has increased  $Q_{dep}$  above  $Q$  by  $16 \pm 6\%$ . Alternatively, we can say that  $14 \pm 4\%$  of  $\text{NH}_3$  emitted from  
516 excretions had been re-deposited to clean patches on the field.

#### 517 **4.2.4 Uncertainty associated with heterogeneous emission patterns**

518 To address the resulting disparity between emission estimates from the downwind concentration receptors  
519 during Period 2, the emission area coefficients (Table 1) were applied to reconcile the independent emission  
520 estimates. This is a valid approach to describe emissions from the field as a whole, as sensor S1 was placed at  
521 the center of the field near the strongest area of emissions, causing emissions to be overestimated as a whole,  
522 while the field area around sensor S3 at the SE corner seems to have contributing very little emissions, hence  
523 causing an underestimation. However, as mentioned previously there are multiple configurations of source area  
524 coefficients which can reconcile  $QS1$  and  $QS3$ . Therefore, a sensitivity test has been carried out to evaluate the  
525 potential error in this method. The numerical solver which derives the source area coefficients contains a  
526 parameter assuming the maximum degree of heterogeneity for the field, where each source area cannot  
527 contribute less than a defined percentage to the overall emissions. This parameter ( $AC_{min}$ ) was varied to provide  
528 differing sets of source area coefficients, yet still reconciling the  $QS1$  and  $QS3$  emission estimates which  
529 was a necessary precondition for the sensitivity test.  $AC_{min}$  was initially assumed be 0.075, 30% of the value for  
530 a homogenous field (0.25), and this value was varied by  $\pm 67\%$  (to 50% and 10% of the homogenous value).  
531 The results of this sensitivity test are given in Table 4, where the percentage change in  $Q_{dep}$  after varying the  
532 parameter by  $+67\%$  and  $-67\%$  was 9 and 1, respectively. The percentage change is greater after increasing  
533  $AC_{min}$  because  $QS1$  and  $QS3$  cannot be reconciled as closely, whereas decreasing  $AC_{min}$  from 0.075 leads to  
534 very little change as the numerical solver can find very close agreement. This suggests that emissions from  
535 excretions to the field are too heterogeneous to assume an  $AC_{min}$  value of 0.125 (50% of homogeneous value),  
536 and that the 1% change in  $Q_{dep}$  after reducing  $AC_{min}$  to 0.025 (10% of homogeneous value) is more indicative  
537 of the uncertainty in the source area optimisation method.

538 The % change in emission estimates was much more sensitive to uncertainty in predicted  $C_b$  than to uncertainty  
539 in  $R_c$  or  $AC_{min}$ . Therefore, we expect that the predicted  $C_b$  ~~to be~~ the greatest source of error in derived fluxes  
540 from the grazed field.

#### 541 **4.3 Temporal variability in estimated emissions**

542 The estimated emissions show significant temporal variability during both measurement periods, typically with  
543 peak emissions occurring during the day with little emissions occurring overnight. Similar diurnal profiles have  
544 been observed in NH<sub>3</sub> emissions from cattle urine and dung patches (Laubach et al., 2012; 2013a), and from  
545 urine patch emission models (Móring et al., 2016). Mechanisms which limit nocturnal emissions can be  
546 summarised as: (1) low wind speeds and stable conditions, which increases the aerodynamic transfer resistances  
547 between the soil/canopy layer and the atmosphere, (2) low temperatures which limit the hydrolysis of urea, and  
548 affect NH<sub>3</sub>/NH<sub>4</sub><sup>+</sup> partitioning in solutions, (3) dew formation on leaf surfaces which act as sinks for NH<sub>3</sub>.

549 A longer temporal trend in emissions is observed during Period 1; with very little emissions occurring on the  
550 first day the cattle were introduced to the field, and peak emissions occurring during the afternoon of the second  
551 day. After 44 cattle had begun to graze the whole field during Period 2, peak emission rates occurred from 22-  
552 23/05, 2-3 days after the cattle had been introduced. A decreasing trend in emissions occurred after the cattle  
553 were removed from the field on 23/05 until the end of the measurement period. This is in-line with the reported  
554 emissions from urine and dung patches by Laubach et al., (2013a), where emissions peaked during the third and  
555 fourth days after grazing had begun, and a following decreasing trend in emissions after the cattle had been  
556 removed from the field on the third day.

557 The peak in emissions which occurred during grazing can be attributed to the hydrolysis of urea within the urine  
558 patches, which leads to a rapid rise in pH and the formation of NH<sub>4</sub><sup>+</sup>, and a high rate of NH<sub>3</sub> volatilisation  
559 (Sherlock and, Goh 1985). As volatilisation proceeds, a subsequent chemical reduction in surface pH occurs  
560 with an accompanying release of a proton to the transformation of NH<sub>4</sub><sup>+</sup> to NH<sub>3</sub> (Laubach et al., 2012; Sherlock  
561 and Goh, 1985, Móring, et al., 2016), which prevents further volatilisation and can explain the declining  
562 emission rate after the cattle had left the field on 23/05.

#### 563 **4.4 Emission factors from the grazing experiment**

564 Emission factors from the grazing experiment have been evaluated as  $6 \pm 2$  and  $7 \pm 2$  g NH<sub>3</sub> cow<sup>-1</sup> d<sup>-1</sup>, and  $9 \pm$   
565  $3\%$  and  $10 \pm 3\%$  of excreted urine-N emitted as NH<sub>3</sub> for the  $Q$  and  $Q_{dep}$  scenarios respectively (average  
566 emission factor  $\pm$  predicted  $C_b$  uncertainty). These emission factors were taken from the Period 2/Scenario 2  
567 estimates as Period 1 was not long enough to fully capture emissions from excretions to the field. Previous  
568 experiments have measured NH<sub>3</sub> emissions from cattle urine patches at ratios of 7-25.7% of excreted urine-N to  
569 grazed pastures (Jarvis et al., 1989; Ryden et al., 1987; Laubach et al., 2012; 2013a). Our estimates for  
570 emissions from grazing are towards the lower end of the range of published emission factors. Differences  
571 between reported emission factors may be related to differing weather conditions affecting the hydrolysis of  
572 urea, or differences in soil properties, where emissions can be limited due to urine percolation into porous soil  
573 (Móring et al., 2016). It is also possible that significant emissions occurred after the miniDOAS instruments had  
574 been removed from the field, which would lead to an underestimation of the proportion of excreted N or urine-N  
575 emitted as NH<sub>3</sub>. The period of significant emissions from urine patches generally lasts 4-8 days after urine  
576 deposition (Sherlock and Goh, 1985; Laubach et al., 2012). However, a rainfall event after a dry period can lead  
577 to a delayed onset of NH<sub>3</sub> emissions by restarting urea hydrolysis (Móring et al., 2016). On the other hand, the  
578 Period 2 emission factors are also influenced to some degree by emissions from excretions during Period 1 on  
579 the SW field, which could cause an overestimation of emissions. Emission factors derived from Period 2 are

580 also affected by  $u^*$  filtering, which may slightly increase estimates due to a measurement bias towards  
581 turbulent daytime periods.

582 The emission estimates presented here show that the ‘gross’ emissions from the field ( $Q_{dep}$  scenario) are around  
583  $16 \pm 6\%$  higher than the ‘net’ emissions ( $Q$  scenario). Both of these estimates are potentially useful to contribute  
584 towards an emission factor for livestock grazing. For example, regional-scale atmospheric dispersion models  
585 may require source inputs as ‘gross’ emission factors due to deposition simulations implicit within the regional-  
586 scale model.

## 587 **5. Conclusion**

588 Fluxes of  $\text{NH}_3$  were estimated through measurement of atmospheric concentrations upwind and downwind of a  
589 grazed field, and applying a bLS dispersion model to simulate the emission rate on a half hourly basis from the  
590 observed horizontal concentration gradient and wind/turbulence measurements. The miniDOAS systems were  
591 well-suited to the task, providing continuous high-time resolution concentration measurements at field  
592 boundaries across the field. Horizontal concentration gradients of  $\sim 0\text{--}9 \mu\text{g m}^{-3}$  were measured between upwind  
593 and downwind receptors. Control on emissions was observed from covariance with temperature, wind speed and  
594 humidity/wetness measurements made on the field, revealing a diurnal emission profile. Two separate  
595 experiments to evaluate emissions were carried out; a Period 1 experiment (2 days) which took place on a small  
596 field with a grazing density of 44 cows  $\text{ha}^{-1}$ , and a Period 2 experiment (10 days) on a larger field with a  
597 grazing density of 22 cows  $\text{ha}^{-1}$ . Spatial heterogeneity in emissions across the field was apparent during Period  
598 2, ~~as a result~~ because of uneven cattle distribution and a low grazing density, adversely affecting the accuracy of  
599 the bLS model estimates. However, after treating the larger field as a grid of discrete source areas the spatial  
600 heterogeneity of emissions was accounted for, by optimising source area coefficients to the measured  
601 concentrations and reconciling emission estimates between downwind receptors.

602 Data gaps in the  $C_b$  measurements were filled by applying linear regression equations with  $u$ ,  $T$  and  $RH$ , which  
603 introduced significant uncertainty into the emission estimates. The evaluated uncertainty in derived emissions  
604 due to  $C_b$  gap-filling was 5% during Period 1 and 31% during Period 2.

605 In contrast to the standard bLS approach, we simulated the effect of re-deposition to unsoiled field patches,  
606 where the canopy resistance ( $R_c$ ) component was estimated by an empirical model derived from local flux and  
607  $R_c$  measurements with  $T$  and  $RH$ . Including deposition in the model increased emissions by  $16 \pm 6\%$ . The  
608 results present both ‘gross’ and ‘net’ emissions from the field, and show that deposition of  $\text{NH}_3$  is an important  
609 consideration when deriving  $\text{NH}_3$  emission factors.

## 610 **Acknowledgements**

611 This study was undertaken as part of the French BtEP project (Emissions gazeuses au Bâtiment, sTockage,  
612 Epandage et Pâturage des systèmes bovins laitiers), convention n° 1360C0032, with funding provided by  
613 ADEME (Agence de l'environnement et de la maîtrise de l'énergie). We wish to thank David Sidaner, Jacques  
614 Lassalas and all of the staff at the INRA-Méjusseume dairy experimental farm. We wish to thank Andi Mórning  
615 for assistance during the measurement campaign. We wish to thank Thomas Kupper for organising the setup of  
616 the N excretion model.

617 **Competing interests**

618 The authors declare that they have no conflict of interest.

619 **References**

- 620 Asman, W. A. H.: Factors influencing local dry deposition of gases with special reference to ammonia,  
621 Atmospheric Environment, 32, 415-421, Doi 10.1016/S1352-2310(97)00166-0, 1998.
- 622 Asman, W. A. H., Sutton, M. A., and Schjorring, J. K.: Ammonia: emission, atmospheric transport and  
623 deposition, New Phytol, 139, 27-48, DOI 10.1046/j.1469-8137.1998.00180.x, 1998.
- 624 Bracher A., Schlegel P., Munger A., Stoll W., Menzi H., 2011. Moglichkeiten zur Reduktion von  
625 Ammoniakemissionen durch Futterungsmassnahmen beim Rindvieh (Milchkuh). Project report Schweizerische  
626 Hochschule fur Landwirtschaft and Agroscope Liebefeld-Posieux for the Swiss Federal Office of Agriculture,  
627 pp. 128, available at: <https://www.blw.admin.ch/blw/de/home/instrumente/ressourcen--und-gewaesserschutzprogramm/ressourcenprogramm.html>, last access: 4 October 2016.
- 628 <https://www.blw.admin.ch/blw/de/home/instrumente/ressourcen--und-gewaesserschutzprogramm/ressourcenprogramm.html>, last access: 4 October 2016.
- 629 Bracher A., Spring P., Munger A., Schlegel P., Stoll W., Menzi H., 2012. Feeding measures to reduce ammonia  
630 emissions. Hassouna M. et al. (Eds), Proc. International Symposium on Emissions of Gas and Dust from  
631 Livestock (EMILI), Saint-Malo 11-13.6.2012, p. 39.
- 632 Carslaw, D. C., and Ropkins, K.: openair - An R package for air quality data analysis, Environ Modell Softw,  
633 27-28, 52-61, 10.1016/j.envsoft.2011.09.008, 2012.
- 634 Erisman, J. W., Sutton, M. A., Galloway, J., Klimont, Z., and Winiwarter, W.: How a century of ammonia  
635 synthesis changed the world, Nat Geosci, 1, 636-639, 10.1038/ngeo325, 2008.
- 636 Famulari, D., Fowler, D., Nemitz, E., Hargreaves, K. J., Storeton-West, R. L., Rutherford, G., Tang, Y. S.,  
637 Sutton, M. A., and Weston, K. J.: Development of a low-cost system for measuring conditional time-averaged  
638 gradients of SO<sub>2</sub> and NH<sub>3</sub>, Environmental Monitoring and Assessment, 161, 11-27, 10.1007/s10661-008-0723-  
639 6, 2010.
- 640 Felber, R., Munger, A., Neftel, A., and Ammann, C.: Eddy covariance methane flux measurements over a  
641 grazed pasture: effect of cows as moving point sources, Biogeosciences, 12, 3925-3940, 10.5194/bg-12-3925-  
642 2015, 2015.
- 643 Flechard, C. R., and Fowler, D.: Atmospheric ammonia at a moorland site. I: The meteorological control of  
644 ambient ammonia concentrations and the influence of local sources, Q J Roy Meteor Soc, 124, 733-757, DOI  
645 10.1002/qj.49712454705, 1998.
- 646 Flechard, C. R., Fowler, D., Sutton, M. A., and Cape, J. N.: A dynamic chemical model of bi-directional  
647 ammonia exchange between semi-natural vegetation and the atmosphere, Q J Roy Meteor Soc, 125, 2611-2641,  
648 DOI 10.1002/qj.49712555914, 1999.
- 649 Flechard, C. R., Spirig, C., Neftel, A., and Ammann, C.: The annual ammonia budget of fertilised cut grassland  
650 - Part 2: Seasonal variations and compensation point modeling, Biogeosciences, 7, 537-556, 2010.
- 651 Flechard, C. R., Massad, R. S., Loubet, B., Personne, E., Simpson, D., Bash, J. O., Cooter, E. J., Nemitz, E., and  
652 Sutton, M. A.: Advances in understanding, models and parameterizations of biosphere-atmosphere ammonia  
653 exchange, Biogeosciences, 10, 5183-5225, 10.5194/bg-10-5183-2013, 2013.

654 Flesch, T. K., Wilson, J. D., and Yee, E.: Backward-Time Lagrangian Stochastic Dispersion Models and Their  
655 Application to Estimate Gaseous Emissions, *J Appl Meteorol*, 34, 1320-1332, Doi 10.1175/1520-  
656 0450(1995)034<1320:Btldsm>2.0.Co;2, 1995.

657 Flesch, T. K., Wilson, J. D., Harper, L. A., Crenna, B. P., and Sharpe, R. R.: Deducing ground-to-air emissions  
658 from observed trace gas concentrations: A field trial, *J Appl Meteorol*, 43, 487-502, Doi 10.1175/1520-  
659 0450(2004)043<0487:Dgefot>2.0.Co;2, 2004.

660 Flesch, T. K., Wilson, J. D., Harper, L. A., and Crenna, B. P.: Estimating gas emissions from a farm with an  
661 inverse-dispersion technique, *Atmospheric Environment*, 39, 4863-4874, 10.1016/j.atmosenv.2005.04.032,  
662 2005.

663 Flesch, T. K., McGinn, S. M., Chen, D., Wilson, J. D., and Desjardins, R. L.: Data filtering for inverse  
664 dispersion emission calculations, *Agr Forest Meteorol*, 198, 1-6, 10.1016/j.agrformet.2014.07.010, 2014.

665 [Fowler, D., Pilegaard, K., Sutton, M. A., Ambus, P., Raivonen, M., Duyzer, J., Simpson, D., Fagerli, H., Fuzzi,](#)  
666 [S., Schjoerring, J. K., Granier, C., Neftel, A., Isaksen, I. S. A., Laj, P., Maione, M., Monks, P. S., Burkhardt, J.,](#)  
667 [Daemmgen, U., Neirynek, J., Personne, E., Wichink-Kruit, R., Butterbach-Bahl, K., Flechard, C., Tuovinen, J.](#)  
668 [P., Coyle, M., Gerosa, G., Loubet, B., Altimir, N., Gruenhage, L., Ammann, C., Cieslik, S., Paoletti, E.,](#)  
669 [Mikkelsen, T. N., Ro-Poulsen, H., Cellier, P., Cape, J. N., Horvath, L., Loreto, F., Niinemets, U., Palmer, P. I.,](#)  
670 [Rinne, J., Misztal, P., Nemitz, E., Nilsson, D., Pryor, S., Gallagher, M. W., Vesala, T., Skiba, U., Brueggemann,](#)  
671 [N., Zechmeister-Boltenstern, S., Williams, J., O'Dowd, C., Facchini, M. C., de Leeuw, G., Flossman, A.,](#)  
672 [Chaumerliac, N., and Erisman, J. W.: Atmospheric composition change: Ecosystems-Atmosphere interactions,](#)  
673 [Atmospheric Environment](#), 43, 5193-5267, 10.1016/j.atmosenv.2009.07.068, 2009.

674 Gao, Z. L., Mauder, M., Desjardins, R. L., Flesch, T. K., and van Haarlem, R. P.: Assessment of the backward  
675 Lagrangian Stochastic dispersion technique for continuous measurements of CH<sub>4</sub> emissions, *Agr Forest*  
676 *Meteorol*, 149, 1516-1523, 10.1016/j.agrformet.2009.04.004, 2009.

677 Genermont, S., and Cellier, P.: A mechanistic model for estimating ammonia volatilization from slurry applied  
678 to bare soil, *Agr Forest Meteorol*, 88, 145-167, Doi 10.1016/S0168-1923(97)00044-0, 1997.

679 Gill Instruments: Technical key note KN1509v3\* - software bug affecting 'w' wind component notice and  
680 available options to customers – February 2016, available at:  
681 [http://gillinstruments.com/data/manuals/KN1509\\_WindMaster\\_WBug\\_info.pdf](http://gillinstruments.com/data/manuals/KN1509_WindMaster_WBug_info.pdf), last access: 4 October 2016.

682 Häni, C.: bLSmodelR - An atmospheric dispersion model in R. R package version 2.4.1. URL:  
683 <http://www.agrammon.ch/documents-to-download/blsmodelr/>, last access: 22 September 2016.

684 Häni, C., Sintermann, J., Jocher, M., Neftel, A.: Ammonia emissions after application of slurry. pp. 168.  
685 Hochschule für Agrar-, Forst- und Lebensmittelwissenschaften, HAFL, Agroscope Institut für  
686 Nachhaltigkeitswissenschaften INH, available at:  
687 <http://www.agrammon.ch/assets/Downloads/SchlussberichtInklAnh20160728subm.pdf>, last access: 4 October  
688 2016.

689 Harper, L. A., Denmead, O. T., and Flesch, T. K.: Micrometeorological techniques for measurement of enteric  
690 greenhouse gas emissions, *Anim Feed Sci Tech*, 166-67, 227-239, 10.1016/j.anifeedsci.2011.04.013, 2011.

691 Hertel, O., Reis, S., Skjøth, C. A., Bleeker, A., Harrison, R., Cape, J. N., Fowler, D., Skiba, U., Simpson, D.,  
692 Jickells, T., Baker, A., Kulmala, M., Gyldenkaerne, S., Sørensen, L. L., and Erisman, J. W.: 2011. Nitrogen  
693 processes in the atmosphere, in: *The European Nitrogen Assessment – Sources, Effects and Policy Perspectives*,

694 edited by Sutton, M. A., Howard, C. M., Erisman, J. W., Billen, G., Grennfelt, P., van Grinsven, H., and  
695 Grizzetti, B., 177–207, Cambridge University Press, Cambridge, UK, 2011.

696 [Kruit, R. J. W., van Pul, W. A. J., Sauter, F. J., van den Broek, M., Nemitz, E., Sutton, M. A., Krol, M., and](#)  
697 [Holtstag, A. A. M.: Modeling the surface-atmosphere exchange of ammonia, Atmospheric Environment, 44,](#)  
698 [945-957, 10.1016/j.atmosenv.2009.11.049, 2010.](#)

699 Hutchings, N. J., Sommer, S. G., Andersen, J. M., and Asman, W. A. H.: A detailed ammonia emission  
700 inventory for Denmark, Atmospheric Environment, 35, 1959-1968, Doi 10.1016/S1352-2310(00)00542-2, 2001.

701 Jarvis, S. C., Hatch, D. J., and Roberts, D. H.: The Effects of Grassland Management on Nitrogen Losses from  
702 Grazed Swards through Ammonia Volatilization - the Relationship to Excretal-N Returns from Cattle, J Agr Sci,  
703 112, 205-216, 1989.

704 Laubach, J., Taghizadeh-Toosi, A., Sherlock, R. R., and Kelliher, F. M.: Measuring and modelling ammonia  
705 emissions from a regular pattern of cattle urine patches, Agr Forest Meteorol, 156, 1-17,  
706 10.1016/j.agrformet.2011.12.007, 2012.

707 Laubach, J., Taghizadeh-Toosi, A., Gibbs, S. J., Sherlock, R. R., Kelliher, F. M., and Grover, S. P. P.: Ammonia  
708 emissions from cattle urine and dung excreted on pasture, Biogeosciences, 10, 327-338, 10.5194/bg-10-327-  
709 2013, 2013a.

710 Laubach, J., Bai, M., Pinares-Patino, C. S., Phillips, F. A., Naylor, T. A., Molano, G., Rocha, E. A. C., and  
711 Griffith, D. W. T.: Accuracy of micrometeorological techniques for detecting a change in methane emissions  
712 from a herd of cattle, Agr Forest Meteorol, 176, 50-63, 10.1016/j.agrformet.2013.03.006, 2013b.

713 Loubet, B., Cellier, P., Milford, C., and Sutton, M. A.: A coupled dispersion and exchange model for short-  
714 range dry deposition of atmospheric ammonia, Q J Roy Meteor Soc, 132, 1733-1763, 10.1256/qj.05.73, 2006.

715 Loubet, B., Asman, W. A. H., Theobald, M. R., Hertel, O., Tang, Y. S., Robin, P., Hassouna, M., Dammgén, U.,  
716 Genermont, S., Cellier, P., and Sutton, M. A.: Ammonia Deposition Near Hot Spots: Processes, Models and  
717 Monitoring Methods, Atmospheric Ammonia, 205-267, Doi 10.1007/978-1-4020-9121-6\_15, 2009.

718 McGinn, S. M., Beauchemin, K. A., Flesch, T. K., and Coates, T.: Performance of a Dispersion Model to  
719 Estimate Methane Loss from Cattle in Pens, J Environ Qual, 38, 1796-1802, 10.2134/jeq2008.0531, 2009.

720 Menzi H., Huguenin O., Muenger A., Schlegel P. Procedure for defining new Swiss standard values for the  
721 nutrient excretions of dairy cows. In Koerner I. et al. (Eds.), Proc. 16th RAMIRAN Conference, Hamburg  
722 Harburg September 8-10 2015, Book of Abstracts, p. 52, 2015.

723 Móríng, A., Vieno, M., Doherty, R. M., Laubach, J., Taghizadeh-Toosi, A., and Sutton, M. A.: A process-based  
724 model for ammonia emission from urine patches, GAG (Generation of Ammonia from Grazing): description and  
725 sensitivity analysis, Biogeosciences, 13, 1837-1861, 10.5194/bg-13-1837-2016, 2016.

726 Pain, B. F., Van der Weerden, T. J., Chambers, B. J., Phillips, V. R., and Jarvis, S. C.: A new inventory for  
727 ammonia emissions from UK agriculture, Atmospheric Environment, 32, 309-313, Doi 10.1016/S1352-  
728 2310(96)00352-4, 1998.

729 R Core Team: R: A language and environment for statistical computing. R Foundation for Statistical  
730 Computing, Vienna, Austria, available at: <https://www.R-project.org/>, last access: 04 October 2016.

731 Reidy, B., Dammgén, U., Dohler, H., Eurich-Menden, B., van Evert, F. K., Hutchings, N. J., Luesink, H. H.,  
732 Menzi, H., Misselbrook, T. H., Monteny, G. J., and Webb, J.: Comparison of models used for national



733 agricultural ammonia emission inventories in Europe: Liquid manure systems, *Atmospheric Environment*, 42,  
734 3452-3464, 10.1016/j.atmosenv.2007.04.009, 2008.

735 Ryden, J. C., Whitehead, D. C., Lockyer, D. R., Thompson, R. B., Skinner, J. H., and Garwood, E. A.:  
736 Ammonia Emission from Grassland and Livestock Production Systems in the Uk, *Environ. Pollut.*, 48, 173-184,  
737 Doi 10.1016/0269-7491(87)90032-7, 1987.

738 Sherlock, R. R., and Goh, K. M.: Dynamics of Ammonia Volatilization from Simulated Urine Patches and  
739 Aqueous Urea Applied to Pasture .1. Field Experiments, *Fert Res*, 5, 181-195, Doi 10.1007/Bf01052715, 1984.

740 Sherlock, R. R., and Goh, K. M.: Dynamics of Ammonia Volatilization from Simulated Urine Patches and  
741 Aqueous Urea Applied to Pasture .2. Theoretical Derivation of a Simplified Model, *Fert Res*, 6, 3-22, Doi  
742 10.1007/Bf01058161, 1985.

743 Sintermann, J., Neftel, A., Ammann, C., Hani, C., Hensen, A., Loubet, B., and Flechard, C. R.: Are ammonia  
744 emissions from field-applied slurry substantially over-estimated in European emission inventories?,  
745 *Biogeosciences*, 9, 1611-1632, 10.5194/bg-9-1611-2012, 2012.

746 Sintermann, J., Dietrich, K., Hani, C., Bell, M., Jocher, M., and Neftel, A.: A miniDOAS instrument optimised  
747 for ammonia field measurements, *Atmos Meas Tech*, 9, 2721-2734, 10.5194/amt-9-2721-2016, 2016.

748 Sommer, S. G., Sogaard, H. T., Moller, H. B., and Morsing, S.: Ammonia volatilization from sows on grassland,  
749 *Atmospheric Environment*, 35, 2023-2032, Doi 10.1016/S1352-2310(00)00428-3, 2001.

750 Sutton, M. A., Fowler, D., and Moncrieff, J. B.: The Exchange of Atmospheric Ammonia with Vegetated  
751 Surfaces .1. Unfertilized Vegetation, *Q J Roy Meteor Soc*, 119, 1023-1045, DOI 10.1002/qj.49711951309,  
752 1993.

753 Sutton, M. A., Howard, C. M., Erisman, J.W., Bealey, W. J., Billen, G., Bleeker, A., Bouwman, A. F., Grennfelt,  
754 P., van Grinsven, H. and Grizzetti, B.: The challenge to integrate nitrogen science and policies: the European  
755 Nitrogen Assessment approach, in: *The European Nitrogen Assessment: Sources, Effects and Policy*  
756 *Perspectives*, edited by: Sutton, M. A., Howard, C. M., Erisman, J. W., Billen, G., Bleeker, A., Grennfelt, P.,  
757 van Grinsven, H., and Grizzetti, B., Cambridge University Press, Cambridge, ISBN 978-1-107-00612-6, 82-96,  
758 2011.

759 Tang, Y. S., Cape, J. N. and Sutton, M. A.: Development and Types of Passive Samplers for 570 Monitoring  
760 Atmospheric NO<sub>2</sub> and NH<sub>3</sub> Concentrations, *Sci. World*, 1, 513–529, Doi:10.1100/tsw.2001.82, 2001.

761 Volten, H., Bergwerff, J. B., Haaima, M., Lolkema, D. E., Berkhout, A. J. C., van der Hoff, G. R., Potma, C. J.  
762 M., Kruit, R. J. W., van Pul, W. A. J., and Swart, D. P. J.: Two instruments based on differential optical  
763 absorption spectroscopy (DOAS) to measure accurate ammonia concentrations in the atmosphere, *Atmos Meas*  
764 *Tech*, 5, 413-427, 10.5194/amt-5-413-2012, 2012.

765 von Bobruzki, K., Braban, C. F., Famulari, D., Jones, S. K., Blackall, T., Smith, T. E. L., Blom, M., Coe, H.,  
766 Gallagher, M., Ghalaieny, M., McGillen, M. R., Percival, C. J., Whitehead, J. D., Ellis, R., Murphy, J., Mohacsi,  
767 A., Pogany, A., Junninen, H., Rantanen, S., Sutton, M. A., and Nemitz, E.: Field inter-comparison of eleven  
768 atmospheric ammonia measurement techniques, *Atmos Meas Tech*, 3, 91-112, 10.5194/amt-3-91-2010, 2010.

769 Whitehead, D. C.: *Grassland Nitrogen*. CAB International, Wallingford, UK, 1995.

770 | [Wesely, M. L., and Hicks, B. B.: A review of the current status of knowledge on dry deposition. \*Atmospheric\*](#)  
771 [Environment, 34, 2261-2282. Doi 10.1016/S1352-2310\(99\)00467-7, 2000.](#)

772 Zaman, M., Sagar, S., Blennerhassett, J. D., and Singh, J.: Effect of urease and nitrification inhibitors on N  
773 transformation, gaseous emissions of ammonia and nitrous oxide, pasture yield and N uptake in grazed pasture  
774 system, *Soil Biol Biochem*, 41, 1270-1280, 10.1016/j.soilbio.2009.03.011, 2009.

775

776

777

778

779

780

781 **Tables**

782 **Table 1: Series of emission coefficients obtained by numerical solving of the difference between *QS1* and *QS3*,**  
 783 **applied to individual emission areas to fit the bLS-R model to concentration measurements on each day. For a grazed**  
 784 **field with homogeneous emissions the emission coefficients for each area would be 0.25. Therefore the emission**  
 785 **coefficients offset the bias in emission estimates between the sensors S1 and S3 by adjusting to the heterogeneity in**  
 786 **emissions across the field area.**

Emission area	20/05	21/05	22/05	23/05	24/05	25/05	26/05	27/05	28/05	29/05
A	0.56	0.31	0.28	0.56	0.36	0.42	0.26	0.21	0.25	0.17
B	0.08	0.14	0.13	0.17	0.18	0.17	0.25	0.25	0.23	0.25
C	0.07	0.07	0.20	0.09	0.19	0.11	0.23	0.28	0.21	0.27
D	0.29	0.47	0.40	0.18	0.26	0.30	0.27	0.26	0.31	0.31

787  
 788  
 789  
 790  
 791  
 792  
 793  
 794  
 795  
 796  
 797  
 798  
 799  
 800  
 801  
 802  
 803  
 804  
 805  
 806  
 807  
 808  
 809  
 810  
 811  
 812  
 813  
 814  
 815

816 **Table 2: Summary table of measurement and modelling results.**

	Period 1			Period 2		
	Scenario <sup>1</sup>	S1	S3	Scenario	S1	S3
$C - C_b$ ( $\mu\text{g NH}_3 \text{ m}^{-3}$ )		1.4	2.1		2.9	1.2
$Q$ ( $\mu\text{g NH}_3 \text{ m}^{-2} \text{ s}^{-1}$ )		0.27	0.29	1	0.27	0.12
				2	0.19	0.16
$Q_{dep}$ ( $\mu\text{g NH}_3 \text{ m}^{-2} \text{ s}^{-1}$ )		0.31	0.34	1	0.31	0.14
				2	0.22	0.19
$Q_{depmax}$ ( $\mu\text{g NH}_3 \text{ m}^{-2} \text{ s}^{-1}$ )		0.33	0.38	1	0.33	0.14
				2	0.24	0.2
$T$ ( $^{\circ}\text{C}$ )		10			14	
$u$ ( $\text{m s}^{-1}$ )		2			1.2	
$RH$ (%)		77			76	
Total Rain (mm)		4.4			0	
$LW$ (% time wet)		84			40	
$R_c$ ( $\text{s m}^{-1}$ )	$Q_{depmax}$	145		$Q_{depmax}$	208	
	$Q_{dep}$	275		$Q_{dep}$	338	
$v_d$ ( $\text{mm s}^{-1}$ )	$Q_{depmax}$	4.4		$Q_{depmax}$	3.2	
	$Q_{dep}$	2.8		$Q_{dep}$	2.2	

<sup>1</sup>Description of model scenarios:  $Q_{dep}$  is the bLS-R emission estimate including dry deposition, with an offset of  $130 \text{ s m}^{-1}$  applied to the  $R_c$  timeseries to account for the limiting of excreted  $\text{NH}_3$  to deposition.  $Q_{depmax}$  is the emission estimate without the offset applied to the  $R_c$  timeseries, and is hence a maximum prediction of the gross emissions from the field. Period 2 emission estimates contain both the original Scenario 1 emission estimates assuming a homogenous field, and the optimised Scenario 2 emission estimates using the area coefficients given in Table 1.

817  
818  
819  
820  
821  
822  
823  
824  
825  
826

827 **Table 3: N excretion model inputs, results, and derived emission factors**

Model Input	Value		Model Output or Emission Factor <sup>1</sup>	Scenario <sup>2</sup>	Value	
	Period 1	Period 2			Period 1	Period 2
Animal Numbers	25	44	N excretion total (kg)		11	40
Animal weight (kg)	650	650	N excretion urine (kg)		8	28
Days since calving	180	183	N excretion faeces (kg)		3	12
Milk yield (kg cow <sup>-1</sup> day <sup>-1</sup> ) <sup>1</sup>	21	22	EF (% total excreted N emitted as NH <sub>3</sub> )	<i>Q</i>	2.5	5.2
				<i>Q<sub>dep</sub></i>	2.9	6
Grass sward: net energy for lactation (MJ kg DM <sup>-1</sup> ) <sup>1</sup>	6.4	6.4	EF (% total excreted urine-N emitted as NH <sub>3</sub> )	<i>Q</i>	2.9	8.9
				<i>Q<sub>dep</sub></i>	4.2	10.4
Grass sward: crude protein content (g kg DM <sup>-1</sup> )	168	168	EF (g NH <sub>3</sub> cow <sup>-1</sup> d <sup>-1</sup> )	<i>Q</i>	5.7	6.2
				<i>Q<sub>dep</sub></i>	6.5	7.2

<sup>1</sup>N excretion calculations are given as the herd total for each measurement period.

<sup>2</sup>*Q* is the net emission rate derived without including deposition in the bLS-R simulation, *Q<sub>dep</sub>* is the gross bLS-R emission estimate including dry deposition, with an *R<sub>c</sub>* offset of 130 s m<sup>-1</sup>. EFs are derived from the S3 flux estimates due to better data coverage during both measurement periods, and Period 2 fluxes are derived from Scenario 2 estimates.

828

829 **Table 4: Sensitivity analysis of the percentage change of the bLS-R gross emission estimates (*Q<sub>dep</sub>*) to variation in**  
 830 **predicted *C<sub>b</sub>* and *R<sub>c</sub>*, and the source area coefficient parameter *AC<sub>min</sub>*.**

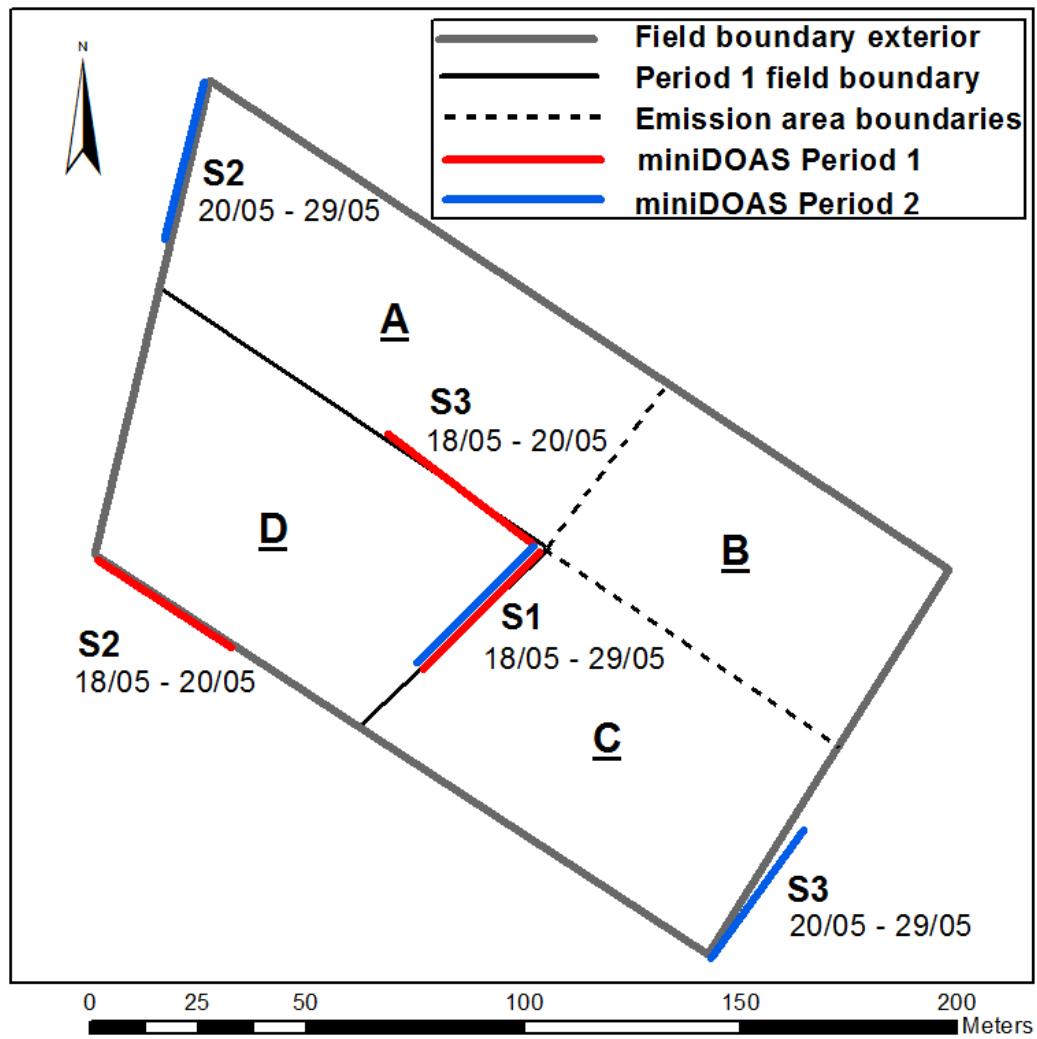
	Period 1	Period 2
<i>C<sub>b</sub></i> data coverage (%)	67	44
<i>C<sub>b</sub></i> MAE (µg m <sup>-3</sup> )	0.33	0.56
% Change <i>C<sub>b</sub></i> ± MAE <sup>1</sup>	-5% +5%	-31% +31%
% Change <i>R<sub>c</sub></i> ± 20%	-2% +3%	-3% +3%
% Change <i>R<sub>c</sub></i> ± 50%	-4% +12%	-5% +5%
% Change <i>AC<sub>min</sub></i> ± 67% <sup>2</sup>	-	-9% -1%

<sup>1</sup>The predicted *C<sub>b</sub>* timeseries input to the bLS-R model is varied by the Mean Absolute Error (MAE) between the measured and predicted *C<sub>b</sub>*. The first value in all cases the % change + variation and the second the % change – variation.

<sup>2</sup> The percentage change in *Q<sub>dep</sub>* is given after varying the source area coefficient parameter *AC<sub>min</sub>* by 67% (0.075 ± 0.05).

831

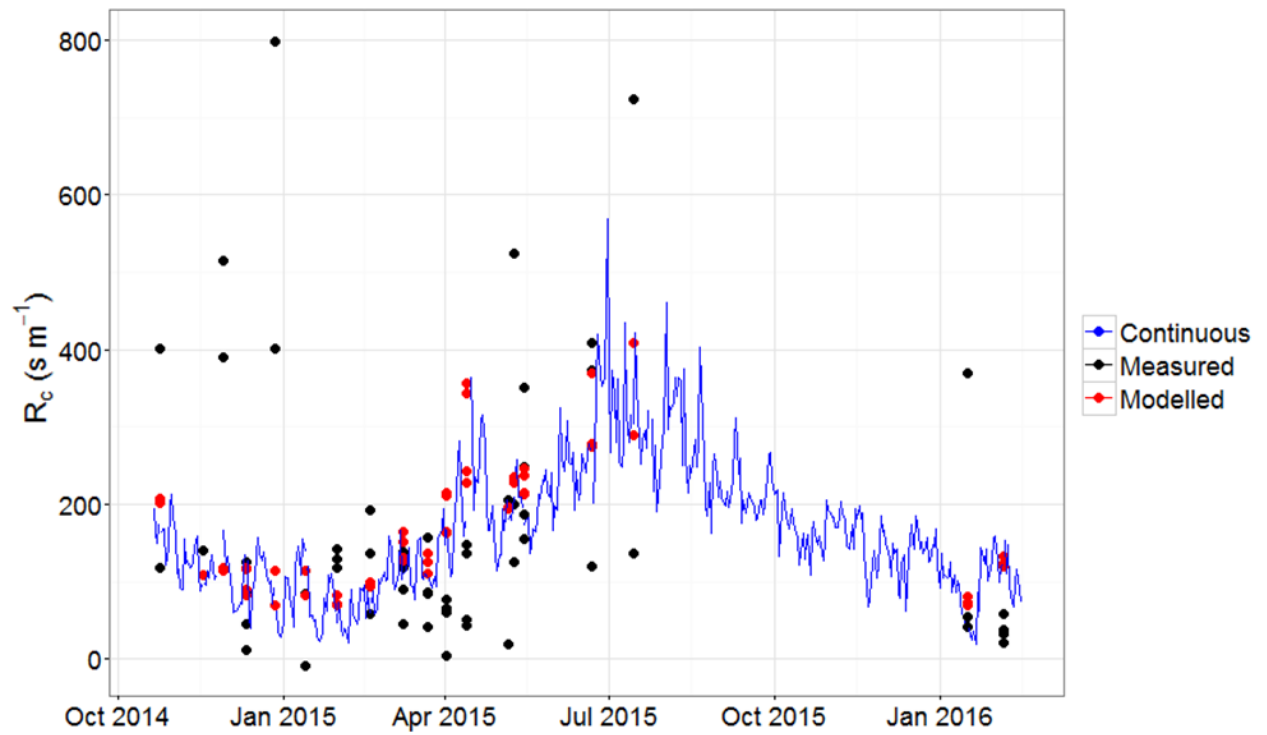
832



834  
 835 **Figure 1: Map of the grazed field showing positions of the three miniDOAS open-path measurement systems. During**  
 836 **Period 1 (18-20/05) 25 cattle were fenced within the SW field section (area D). During Period 2 (20-29/05) the internal**  
 837 **field boundaries were removed so that the cattle could graze the whole field. Later, for the attribution of emissions**  
 838 **across the field, emission area quadrants have been allocated, marked A-D. There were no physical barriers between**  
 839 **the emission areas during Period 2.**

840

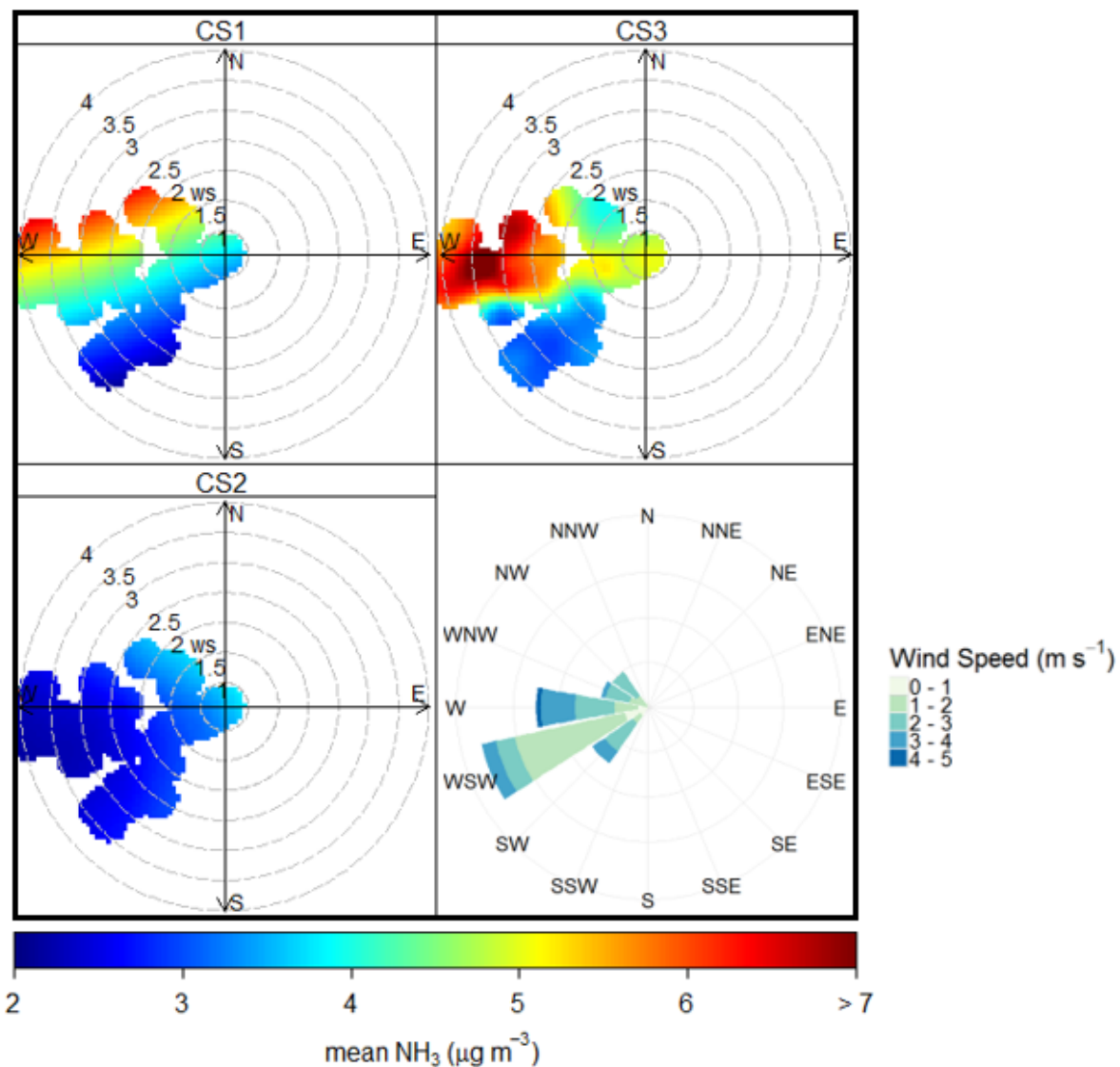
841



842

843 **Figure 2: Timeseries of time-integrated COTAG  $R_c$  measurements and Equation 4  $R_c$  estimates. The blue line**  
 844 **represents continuous  $R_c$  estimates calculated from the daily mean  $T$  and  $RH$  measurements at the field site. Black**  
 845 **points are the measured  $R_c$  values from the COTAG systems, and the red points are the modelled  $R_c$  from the same**  
 846 **time-integrated data.**

847



848

849 **Figure 3: Polar plots showing averaged NH<sub>3</sub> concentrations (colour axis) as a function of wind speed (radial axis) and**  
 850 **wind direction (cardinal direction) for each miniDOAS system, and a windrose showing the prevailing wind**  
 851 **direction, Period 1 (18-20/05). The concentration Polar plots were produced using the OpenAir R package (Carslaw**  
 852 **et al., 2014).**

853

854

855

856

857

858

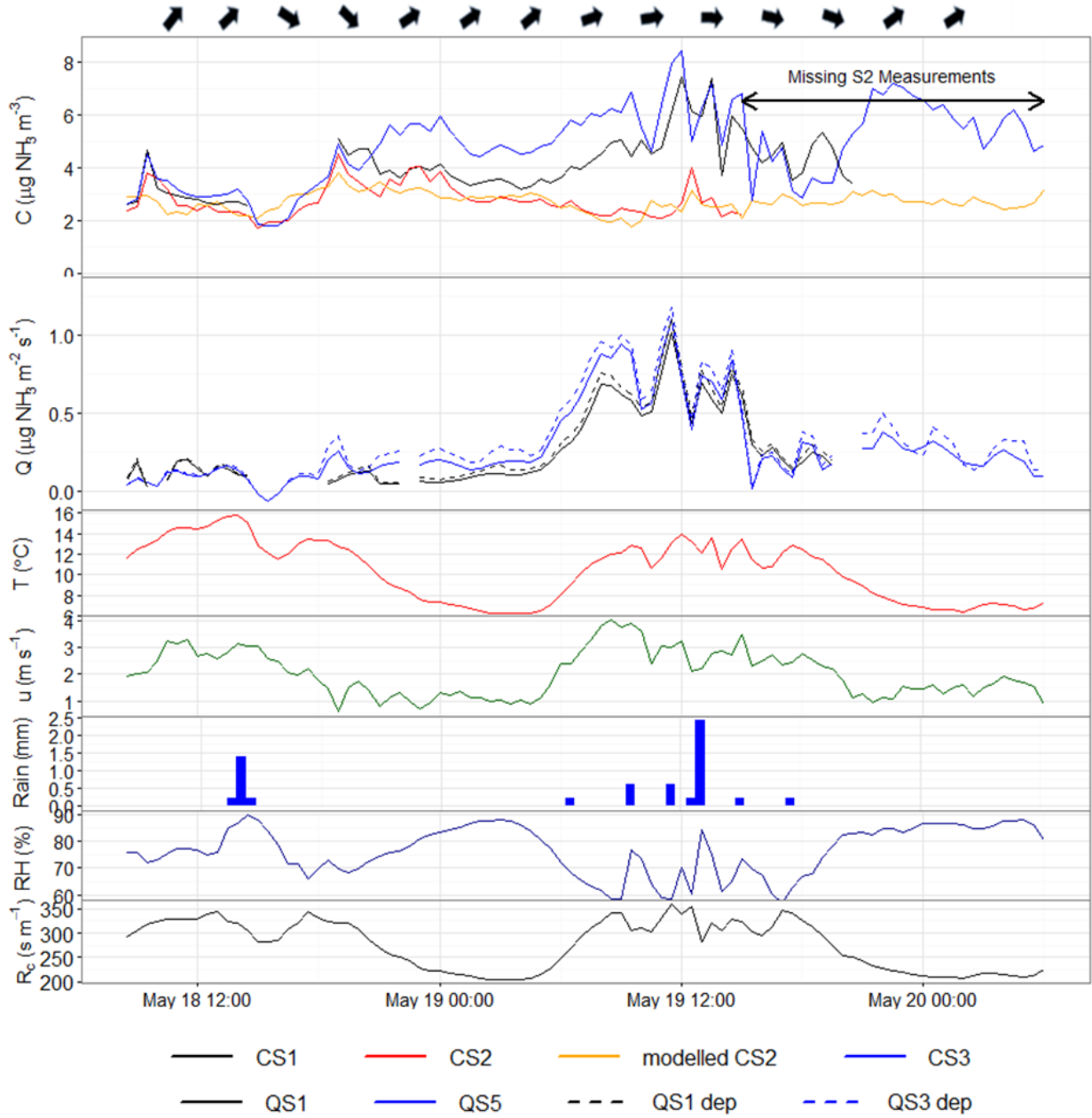
859

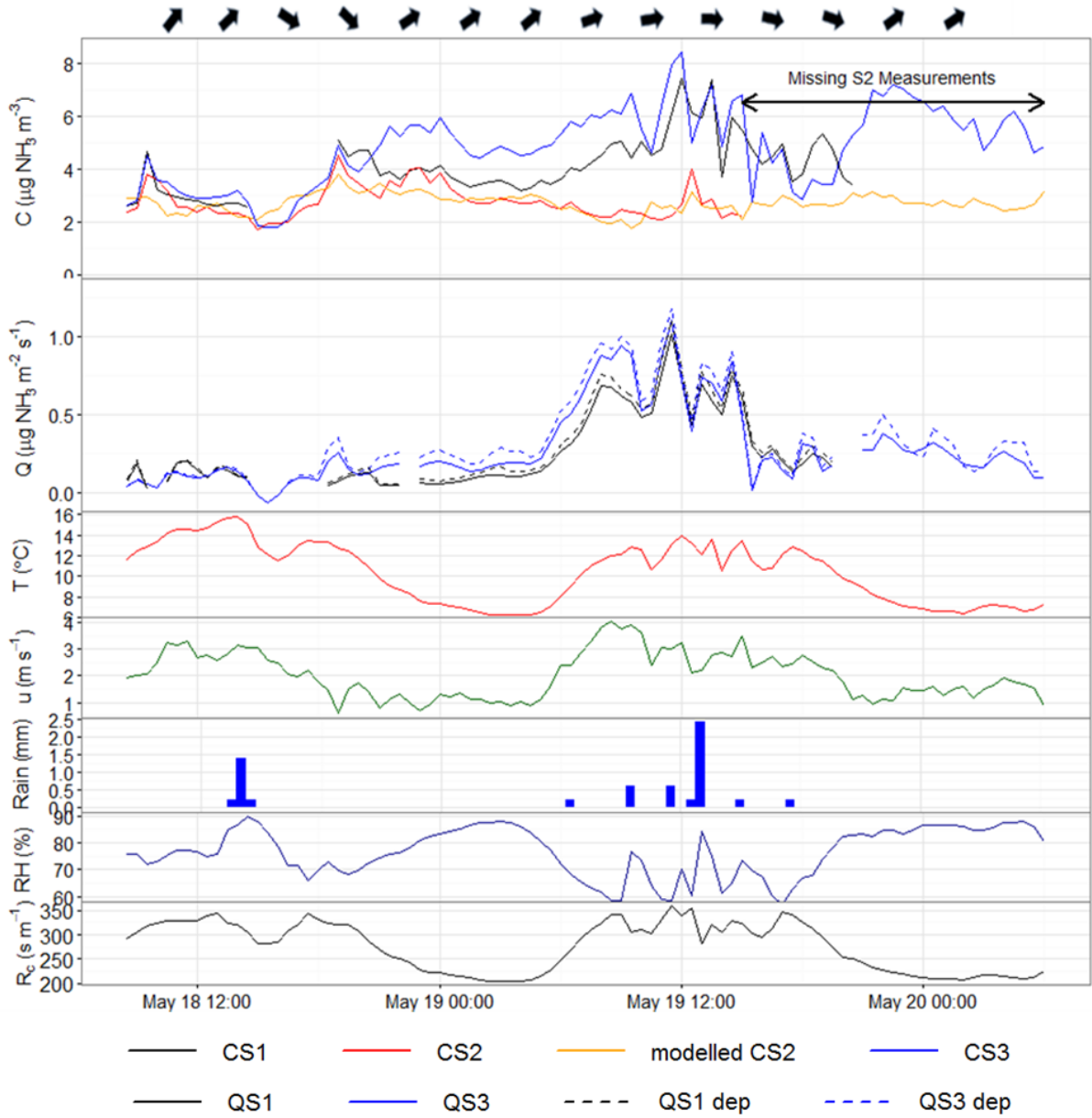
860

861

862

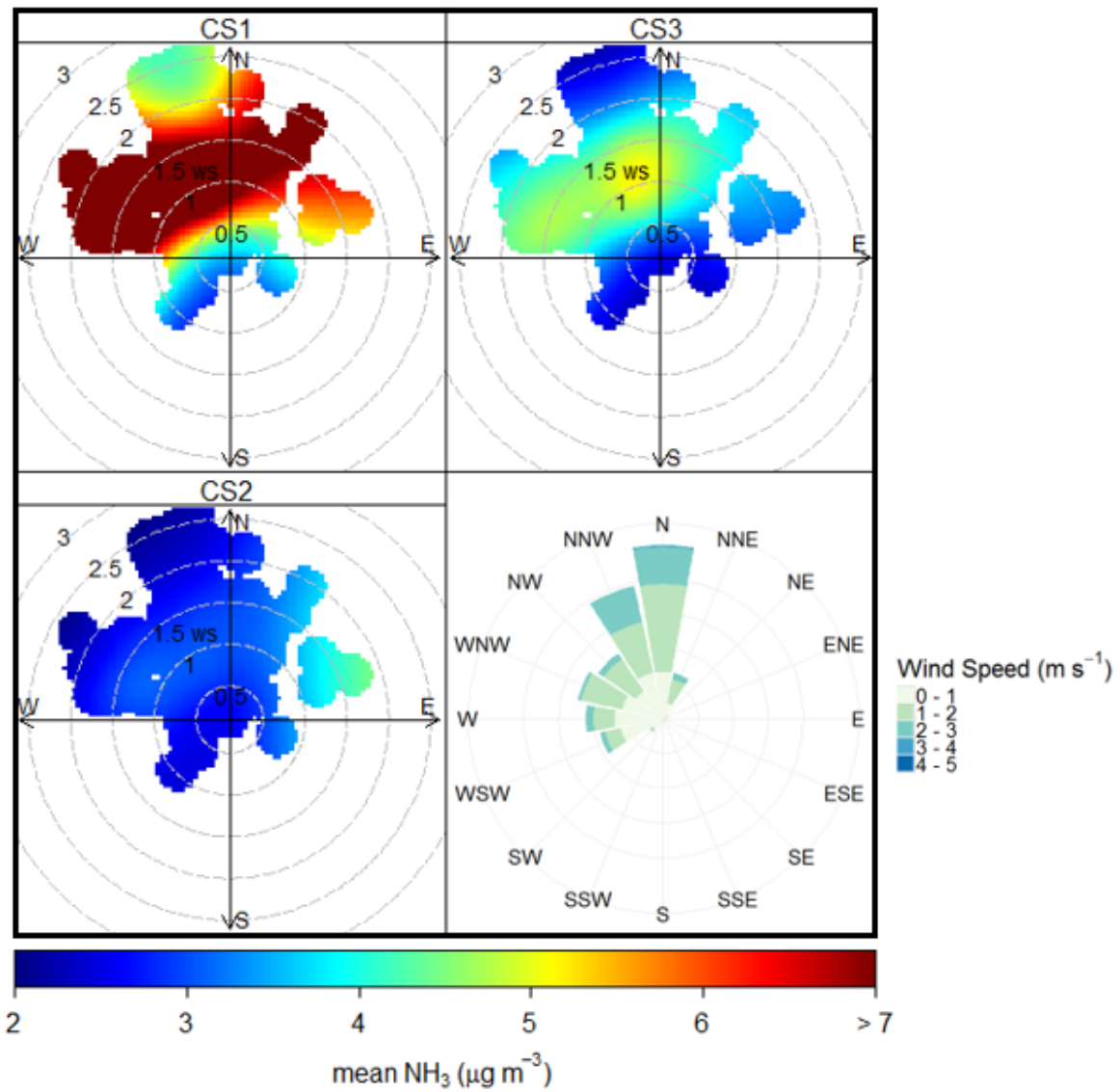






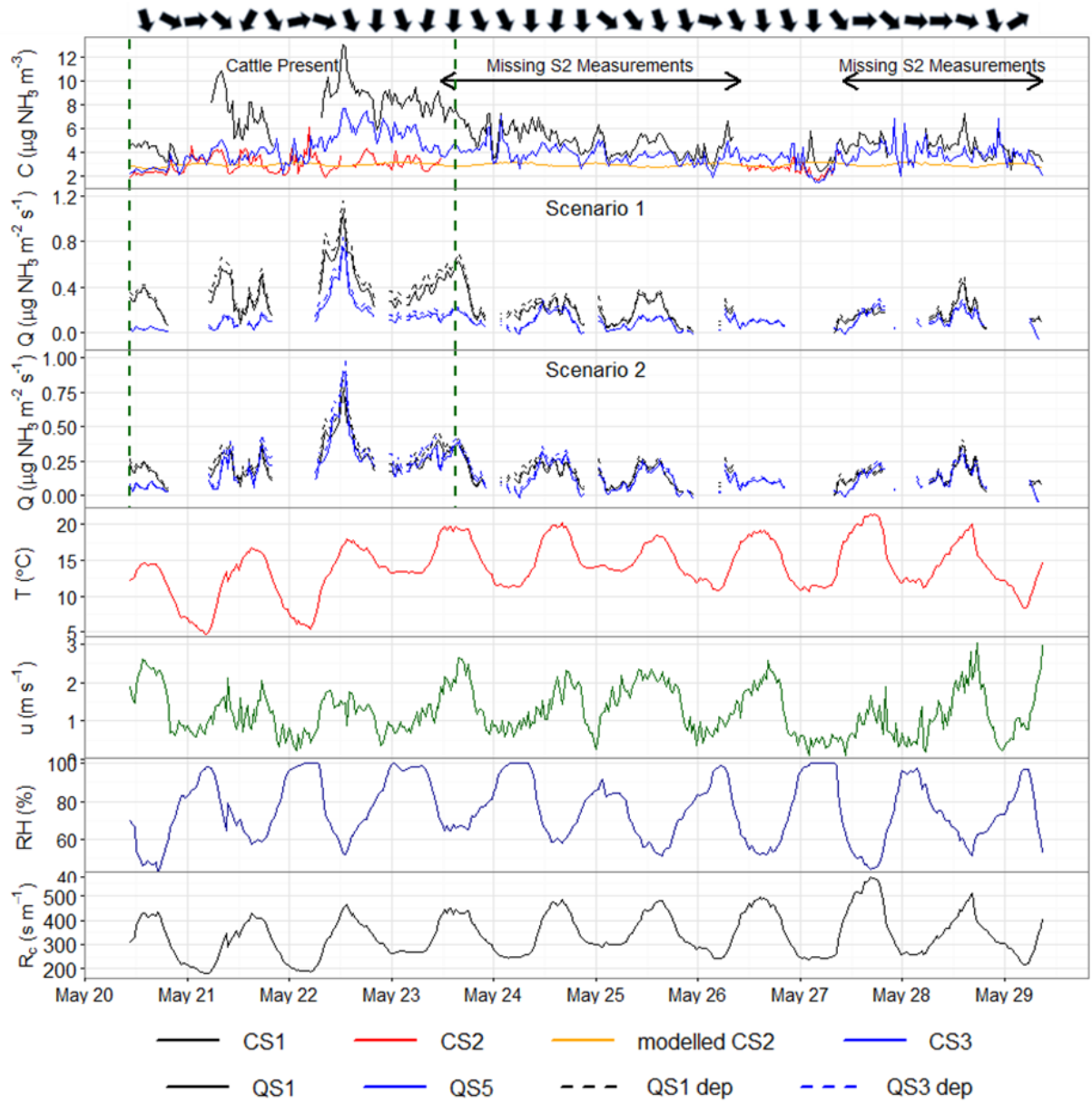
864

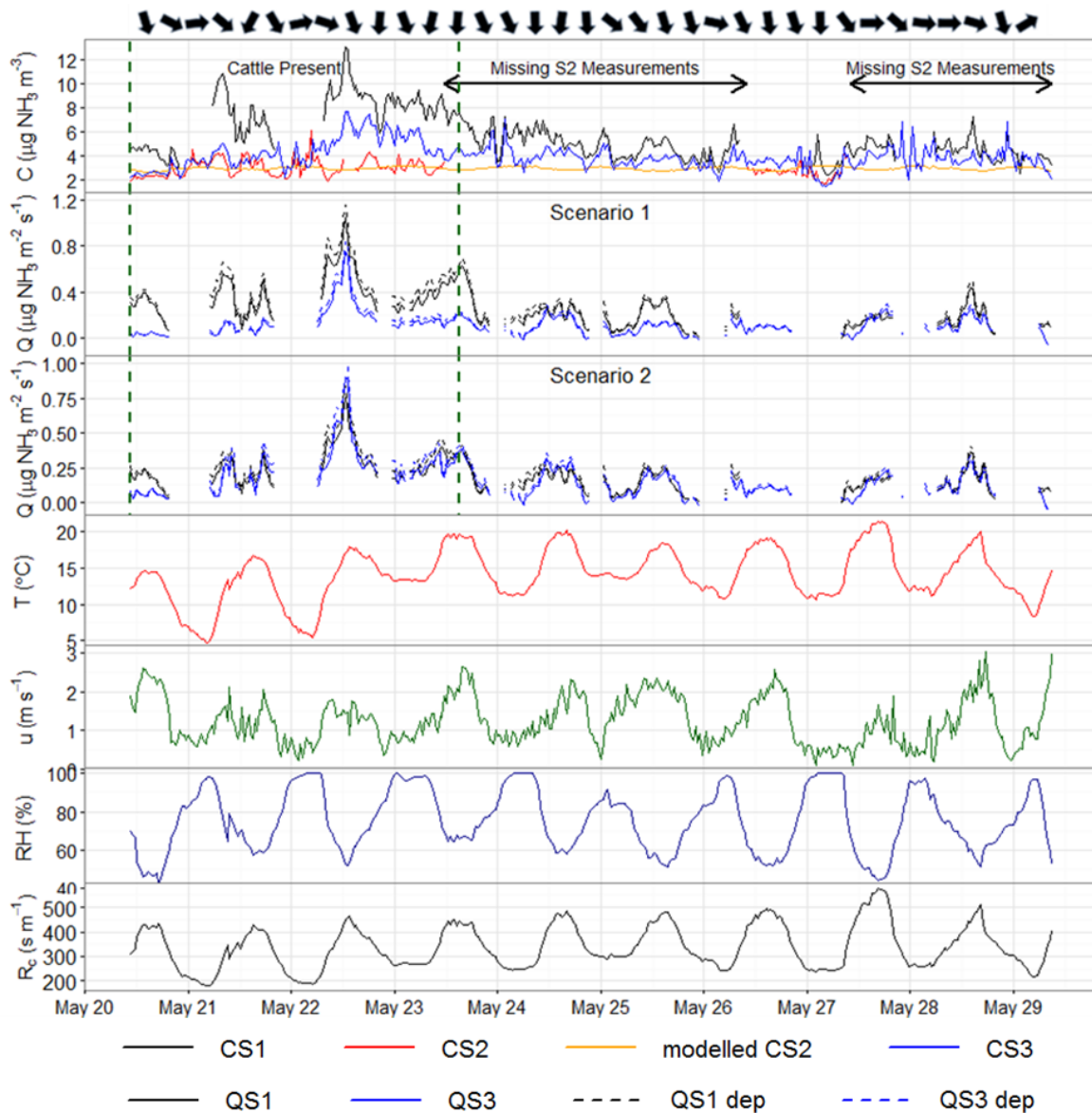
865 **Figure 4: Timeseries of Period 1 DOAS concentration measurements (CS1, CS2, CS3, and modelled CS2 using**  
 866 **Equation 6, top panel) and bLS-R emission estimates (Q and  $Q_{dep}$  scenarios, second panel), with  $T$ ,  $u$ , Rain,  $RH$ , and**  
 867 **modelled  $R_c$  using Equation 5 shown in the panels below. Wind direction arrows are set above the top panel to**  
 868 **visualise changes over time. The cattle were present on the field for the full time period shown (08:00 18/05 - 15:00**  
 869 **20/05).**



870

871 **Figure 5: Polar plots showing averaged  $\text{NH}_3$  concentrations with wind speed and direction for each DOAS system,**  
 872 **with a windrose showing the prevailing wind directions, Period 2 (20-29/05).**





874

875 **Figure 6: Timeseries of Period 2 DOAS concentration measurements (top panel) and bLS-R emission estimates**  
 876 **(second and third panels, showing the  $Q$  (solid lines) and  $Q_{dep}$  (dashed lines) scenarios); with  $T$ ,  $u$ ,  $RH$ , and  $R_c$  (with**  
 877 **130 s m<sup>-1</sup> offset) shown in the panels below. The second panel shows the Scenario 1 (homogenous field) emission**  
 878 **estimates, while the third panel contains the optimised Scenario 2 estimates using the heterogeneous source area**  
 879 **coefficients given in Table 1. Periods with missing S2 background concentration measurements are annotated on the**  
 880 **top panel to highlight the higher uncertainty of these periods for emission estimates. Wind direction arrows are set**  
 881 **above the top panel to visualise changes over time. The dashed green lines on the top panels mark the 3-day time**  
 882 **period where the cattle were grazing the field.**

883